

5-22-2017

Rock magnetic and geochemical evidence for authigenic magnetite formation via iron reduction in coal-bearing sediments offshore Shimokita Peninsula, Japan (IODP Site C0020)

Stephen C. Phillips

University of New Hampshire, Durham

Joel E. Johnson

University of New Hampshire, Durham, joel.johnson@unh.edu

William C. Clyde

University of New Hampshire, Durham, Will.Clyde@unh.edu

Jacob B. Setera

University of New Hampshire, Durham

Daniel P. Maxbauer

University of Minnesota

See next page for additional authors

Follow this and additional works at: https://scholars.unh.edu/faculty_pubs

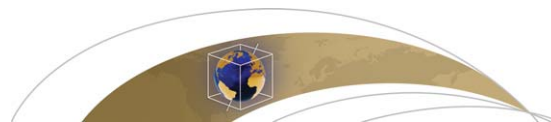
Recommended Citation

Phillips, S.C., Johnson, J.E., Clyde, W.C., Setera, J.B., Maxbauer, D.P., Severmann, S., and Riedinger, N., 2017. Rock magnetic and geochemical evidence for authigenic magnetite formation via iron reduction in coal-bearing sediments offshore Shimokita Peninsula, Japan (IODP Site C0020). *Geochemistry, Geophysics, Geosystems*, v. 18, i 6, pp. 2076–2098. <http://onlinelibrary.wiley.com/doi/10.1002/2017GC006943/abstract>

This Article is brought to you for free and open access by University of New Hampshire Scholars' Repository. It has been accepted for inclusion in Faculty Publications by an authorized administrator of University of New Hampshire Scholars' Repository. For more information, please contact nicole.hentz@unh.edu.

Authors

Stephen C. Phillips, Joel E. Johnson, William C. Clyde, Jacob B. Setera, Daniel P. Maxbauer, Silke Severmann,
and Natascha Riedinger



RESEARCH ARTICLE

10.1002/2017GC006943

Key Points:

- Increased magnetic susceptibility was observed associated with a deeply buried (~2 km) coal-bearing unit
- Rock magnetic/geochemical properties indicate that fine-grained magnetite within the coal-bearing unit increases magnetic susceptibility
- Peat/lignite was likely source of electron donors during burial to fuel production of fine-grained, authigenic magnetite via iron reduction

Supporting Information:

- Supporting Information S1
- Table S1
- Table S2
- Table S3
- Table S4

Correspondence to:

S. C. Phillips,
phillips.stephen.c@gmail.com

Citation:

Phillips, S. C., J. E. Johnson, W. C. Clyde, J. B. Setera, D. P. Maxbauer, S. Severmann, and N. Riedinger (2017), Rock magnetic and geochemical evidence for authigenic magnetite formation via iron reduction in coal-bearing sediments offshore Shimokita Peninsula, Japan (IODP Site C0020), *Geochem. Geophys. Geosyst.*, 18, 2076–2098, doi:10.1002/2017GC006943.



Received 31 MAR 2017

Accepted 8 MAY 2017

Accepted article online 22 MAY 2017

Published online 14 JUN 2017

Rock magnetic and geochemical evidence for authigenic magnetite formation via iron reduction in coal-bearing sediments offshore Shimokita Peninsula, Japan (IODP Site C0020)

Stephen C. Phillips^{1,2} , Joel E. Johnson¹ , William C. Clyde¹ , Jacob B. Setera^{1,3}, Daniel P. Maxbauer^{4,5}, Silke Severmann⁶, and Natascha Riedinger^{7,8}

¹Department of Earth Sciences, University of New Hampshire, Durham, New Hampshire, USA, ²Now at Institute for Geophysics, Jackson School of Geosciences, University of Texas at Austin, Austin, Texas, USA, ³Now at Department of Earth and Planetary Sciences, Rutgers University, Piscataway, New Jersey, USA, ⁴Department of Earth Sciences, University of Minnesota, Minneapolis, Minnesota, USA, ⁵Institute for Rock Magnetism, University of Minnesota, Minneapolis, Minnesota, USA, ⁶Department of Marine and Coastal Sciences, Rutgers University, New Brunswick, New Jersey, USA, ⁷Department of Earth Sciences, University of California-Riverside, California, USA, ⁸Now at Boone Pickens School of Geology, Oklahoma State University, Stillwater, Oklahoma, USA

Abstract Sediments recovered at Integrated Ocean Drilling Program (IODP) Site C0020, in a fore-arc basin offshore Shimokita Peninsula, Japan, include numerous coal beds (0.3–7 m thick) that are associated with a transition from a terrestrial to marine depositional environment. Within the primary coal-bearing unit (~2 km depth below seafloor) there are sharp increases in magnetic susceptibility in close proximity to the coal beds, superimposed on a background of consistently low magnetic susceptibility throughout the remainder of the recovered stratigraphic sequence. We investigate the source of the magnetic susceptibility variability and characterize the dominant magnetic assemblage throughout the entire cored record, using isothermal remanent magnetization (IRM), thermal demagnetization, anhysteretic remanent magnetization (ARM), iron speciation, and iron isotopes. Magnetic mineral assemblages in all samples are dominated by very low-coercivity minerals with unblocking temperatures between 350 and 580°C that are interpreted to be magnetite. Samples with lower unblocking temperatures (300–400°C), higher ARM, higher-frequency dependence, and isotopically heavy $\delta^{56}\text{Fe}$ across a range of lithologies in the coal-bearing unit (between 1925 and 1995 mbsf) indicate the presence of fine-grained authigenic magnetite. We suggest that iron-reducing bacteria facilitated the production of fine-grained magnetite within the coal-bearing unit during burial and interaction with pore waters. The coal/peat acted as a source of electron donors during burial, mediated by humic acids, to supply iron-reducing bacteria in the surrounding siliciclastic sediments. These results indicate that coal-bearing sediments may play an important role in iron cycling in subsiding peat environments and if buried deeply through time, within the subsequent deep biosphere.

1. Introduction

Iron cycling is thought to be an important component within the deep biosphere and the microbial processes and iron phase transformations occurring within deep sedimentary sequences remain an area of active investigation [e.g., Lovley and Chapelle, 1995; D'Hondt et al., 2004; Riedinger et al., 2010]. Rock magnetic studies of buried petroleum hydrocarbon systems indicate iron oxide and sulfide precipitation associated with these deposits [e.g., McCabe et al., 1987; Sassen et al., 1989; Elmore et al., 1997]. However, iron cycling and authigenic magnetic mineral assemblages in deeply buried coal systems are less understood. Peat precursors to coal formation are host to active iron cycling during early burial [e.g., Altschuler et al., 1983; Holmer et al., 1994; Steinmann and Shoty, 1997], but after burial, coal beds are generally considered devoid of bioavailable iron [Strapoć et al., 2011]; however, coal bed methane production may be influenced by iron availability [Ünal et al., 2012]. Application of rock magnetic techniques to scientific drilling records can provide insight into iron cycling within subsiding peat/coal sequences, and the evolution of authigenic iron oxides and sulfides in these systems during burial.

Rock magnetic properties of sedimentary sequences can reveal information about the composition and grain size of magnetic mineral assemblages, which often facilitates the interpretation of depositional and/or diagenetic processes [Verosub and Roberts, 1995; Liu et al., 2012; Roberts, 2015]. In marine deposits, common magnetic minerals include (titano)magnetite ($\text{Fe}_{3-x}\text{Ti}_x\text{O}_4$), hematite (Fe_2O_3), goethite (FeOOH), greigite (Fe_3S_4), and pyrrhotite (Fe_7S_8). Each of these minerals is suggestive of different depositional and/or diagenetic conditions and each can be identified using common rock magnetic techniques. For instance, detrital iron oxides like (titano)magnetite, hematite, and goethite are often formed on continents and then transported to marine sediments via fluvial [e.g., Canfield, 1997], eolian [e.g., Robinson, 1986; Bloemendal et al., 1993; Mahowald et al., 2005; Fan et al., 2006], and ice-rafted debris [e.g., Hall and King, 1989; Richter et al., 2001] transport. Fine-grained authigenic magnetite can also be produced directly by magnetotactic bacteria in deep marine and coastal environments [e.g., Kirschvink and Chang, 1984; Karlin et al., 1987; Roberts et al., 2011]. In anoxic sediments, magnetic iron oxides are common and subject to dissolution and replacement by pyrite [e.g., Canfield and Berner, 1987; Karlin, 1990; Canfield et al., 1992; Poulton et al., 2004; Garming et al., 2005; Riedinger et al., 2005]. Iron sulfides like greigite and pyrrhotite form as an intermediate step during pyrite formation in anoxic environments [e.g., Sweeney and Kaplan, 1973; Furukawa and Barnes, 1995; Neretin et al., 2004] and are generally indicative of sulfur-limiting conditions, such as those present in gas hydrate-bearing settings [e.g., Housen and Musgrave, 1996; Larrasoana et al., 2006, 2007; Musgrave et al., 2006; Fu et al., 2008; Kars and Kodama, 2015]. Microbial reduction of amorphous ferric iron oxides in anoxic environments often results in the precipitation of extracellular magnetite [Lovley et al., 1987]. Additionally, crystalline magnetic Fe(III)-bearing oxides, such as hematite, goethite, and magnetite, may directly serve as a source of Fe(III) electron acceptors for iron-reducing bacteria [e.g., Arnold et al., 1988; Lovley, 1991a; Kostka and Nealson, 1995; Byrne et al., 2015].

Often, marine sediments contain multiple populations of detrital magnetic minerals that record sources and diagenetic processes that affect the preserved magnetic mineral assemblage [e.g., Larrasoana et al., 2007; Just et al., 2012; Ludwig et al., 2013; Kars and Kodama, 2015]. Magnetic mineral diagenesis, however, is generally influenced by depositional setting. For example, in marine environments, the diffusion of seawater sulfate into near-seafloor sediments serves as an electron acceptor for sulfate reduction, and this increases the potential for the formation of pyrite and/or greigite. Similarly, iron oxides are also consumed by reaction with hydrogen sulfide or microbial iron reduction. In contrast, in freshwater environments, where sulfate concentrations are typically 2–3 orders of magnitude lower, iron is a more prevalent electron acceptor [Nealson and Saffarini, 1994].

In this study, we use the rock magnetic properties to characterize ferrimagnetic mineral phases within a deeply buried (1.2–2.5 km) interval of sediment recovered by the *D/V Chikyu* in an ocean drilling record (IODP Hole C0020A) in the Hidaka Trough offshore Shimokita Peninsula, Japan (Figure 1). Within this record, we utilize magnetic susceptibility, coercivity, unblocking temperature, iron speciation, and iron isotopic measurements to identify dominant magnetic mineral assemblages and discuss their origin, while also evaluating their potential role in iron and carbon cycling during burial at this site in association with the subsurface coal beds [Inagaki et al., 2015].

2. Geological Setting

IODP Site C0020A (Figure 1) is located in a fore-arc basin formed as a result of the subduction of the Pacific plate beneath northeast Honshu [Von Huene et al., 1982; Sacks and Suyehiro, 2003]. Fore-arc basin subsidence offshore Shimokita has been occurring since the Cretaceous, and through time the interaction between subsidence and eustatic sea level change has significantly modified the continental margin depositional environment [Von Huene et al., 1982]. Rates of fore-arc subsidence in northeast Honshu since the Miocene correspond to changes in regional plate boundary dynamics [Regalla et al., 2013]. The late Oligocene to early Miocene sediments within the basin record a broad transition in the depositional environment from a terrestrial to marginal marine setting and the sediments from the Neogene to present represent a marginal marine to open marine transition [Arthur et al., 1980; Von Huene et al., 1982]. Previous drilling during Deep Sea Drilling Project Legs 56, 57, and 58 and Ocean Drilling Program (ODP) Leg 186 along the Japan Trench offshore northern Honshu (seaward of IODP Site C0020A) revealed Cretaceous to Holocene

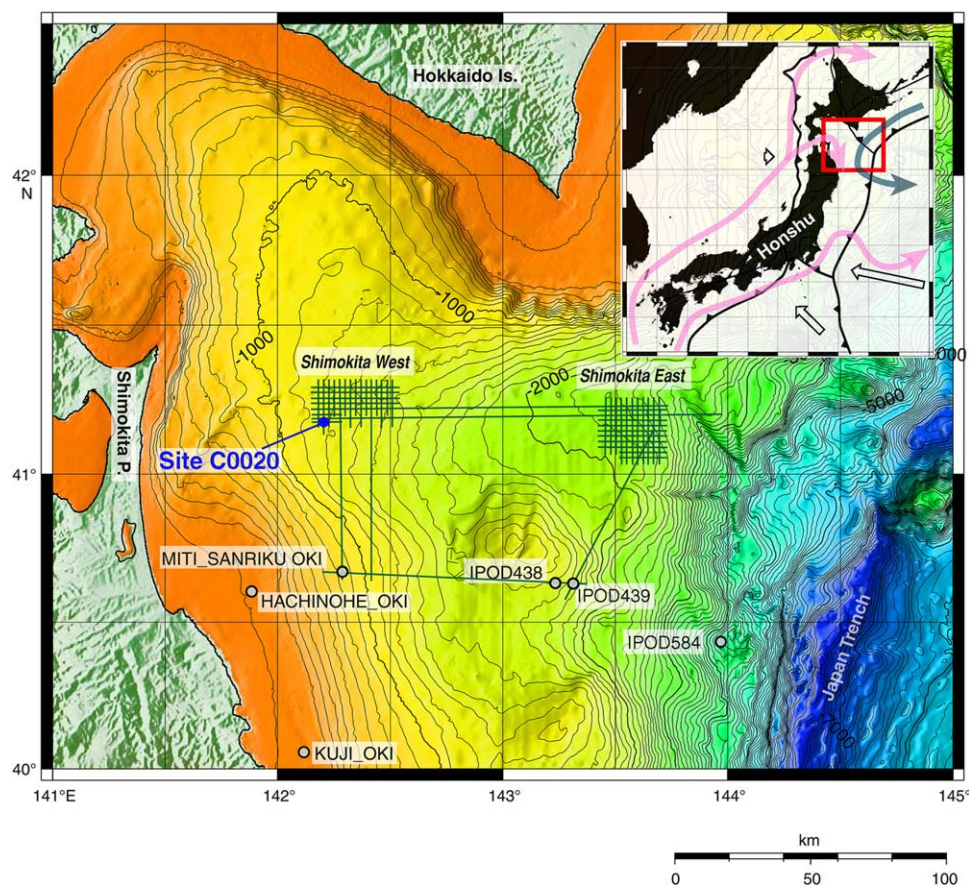


Figure 1. Bathymetric map with the location of Site C0020A along with the location of previous Deep Sea Drilling Project (DSDP) drilled during the International Phase of Ocean Drilling (IPOD Sites 438, 439, 584) and industry holes (Miti Sanriku Oki, Hachinohe Oki, Kuji Oki) drilled offshore Shimokita. Inset shows plate tectonic configuration and plate motions. Open arrows indicate plate motions, pink arrows indicate modern warm currents, and the blue arrow indicates modern cold currents. Modified from *Expedition 337 Scientists* [2013].

sediments primarily composed of hemipelagic clay containing lithic fragments, siliceous/calcareous microfossils, volcanic ash/pumice, and turbidites [Arthur *et al.*, 1980].

3. Site C0020 Lithostratigraphy

The cores recovered onboard the *D/V Chikyu* at IODP Site C0020 are subdivided into four main lithostratigraphic units that are defined from macroscopic and microscopic description of core cuttings and sediment cores. The sediments in these strata record a transition from a late Oligocene/early Miocene terrestrial wetland environment to a Pleistocene marine continental slope sedimentary environment (Figure 2) [Expedition 337 Scientists, 2013; Phillips *et al.*, 2016]. Unit I (636.5–1256.5 mbsf; late Pliocene to Miocene) is composed of diatom-rich silty clay consistent with a continental slope hemipelagic environment. No cores were recovered from Unit I and all descriptions were made from cuttings. Unit II (1256.5–1826.5 mbsf; Miocene) comprises lithified silty shale, siltstone, sandstone, and unconsolidated sand. Observations of *Cruziana* ichnofacies and symmetric wave-formed ripples, along with an increase in glauconite and plant material, suggest the transition to a continental shelf and nearshore environment within Unit II [Expedition 337 Scientists, 2013]. Lignite fragments were observed in cuttings in Unit II between 1526.5 and 1546.5 mbsf and downhole logging identified three coal beds, ranging from 0.3 to 0.9 m in thickness suggesting a nearshore environment [Expedition 337 Scientists, 2013]. Unit III (1826.5–2046.5 mbsf; early Miocene to late Oligocene) contains numerous coal beds interbedded with sandstones (some cemented), siltstones, and coaly shale with common authigenic siderite nodules (1–9 cm thick). These coal beds range from 0.3 to 7.3 m in thickness and comprise low-maturity lignite to subbituminous coal, increasing in maturity with depth [Gross *et al.*, 2015]. Geochemical and petrological analyses of Unit III coal indicate a shift from peat deposited in a

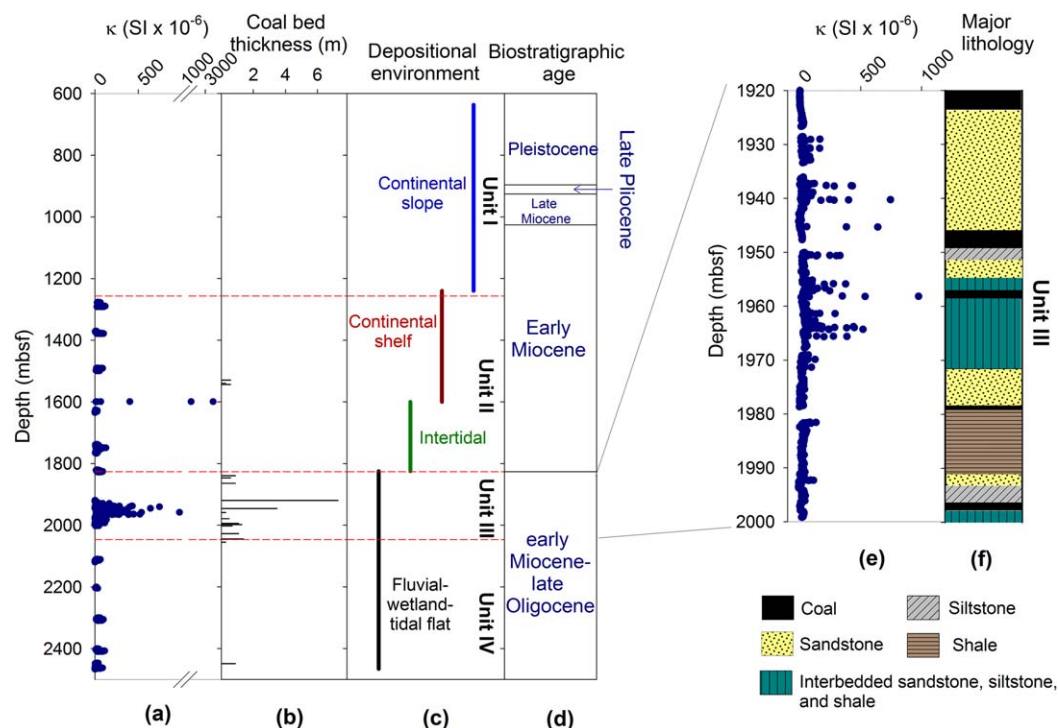


Figure 2. Shipboard measurements of (a) volume-specific magnetic susceptibility, (b) coal thickness, (c) depositional environment, and (d) biostratigraphic age for IODP Hole C0020A. (e) Expanded view of shipboard measurements of volume-specific magnetic susceptibility in Unit III with a simplified stratigraphic column of Unit III (f). Data from *Expedition 337 Scientists* [2013] with updated biostratigraphy from *Phillips et al.* [2016].

freshwater, neutral-to-slightly-acidic environment at the bottom of Unit III to a brackish, and alkaline environment at the top of Unit III [Gross *et al.*, 2015]. Dark-colored, organic-rich mm-scale laminations occur within sandstone and siltstone within Unit III. Flaser and lenticular bedding, cross-bedding, and extensive bioturbation present within Unit III suggest a nearshore to estuarine/intertidal environment [Expedition 337 Scientists, 2013]. Unit IV (2046.5–2466 mbsf; early Miocene) is comprised of silty shale, sandstone, and siltstone, with common siderite nodules (1–3 cm thickness). Fluctuations between fine and coarse-grained beds suggest tidal flats and channels within a fluviodeltaic system [Expedition 337 Scientists, 2013]. Unit IV is mostly devoid of coal beds, except for a 0.9 m thick coal bed with a pyrite vein at 2448 mbsf, near the bottom of the hole.

There are cm-scale increases in volume-specific magnetic susceptibility (κ , SI) (see section 4.2) in Unit III between 1919 and 1970 mbsf (Figure 2). The increases in κ , up to 975×10^{-6} SI from a background of $15.5 \pm 31.9 \times 10^{-6}$ SI occur in sediments adjacent to, but rarely within, the massive coal beds. The increases in κ within this interval occur over intervals that are several-to-tens of cm thick and often are associated with intervals containing dark, organic-rich laminations (Figure 3). There is an additional sharp increase in κ in Unit II at 1599.0–1599.16 mbsf associated with a coarse-grained gravel interval containing rounded pebbles and cobbles of igneous rock [Expedition 337 Scientists, 2013].

4. Methods

4.1. Sample Preparation

Onboard *D/V Chikyu*, bulk sediment and rock samples between 10 and 20 cm³ were sampled for magnetic analyses either from working half sections or whole round core sections from microbiology sampling [see Expedition 337 Scientists, 2013], flushed with nitrogen and vacuum-sealed. No samples were collected from drill cuttings. The working half samples were chosen based on the downhole pattern in shipboard κ measurements and to be representative of recovered lithologies. Whole round samples were recovered at regular intervals down core. Samples were stored at sea and shipped at 2°C, and then stored in the laboratory at

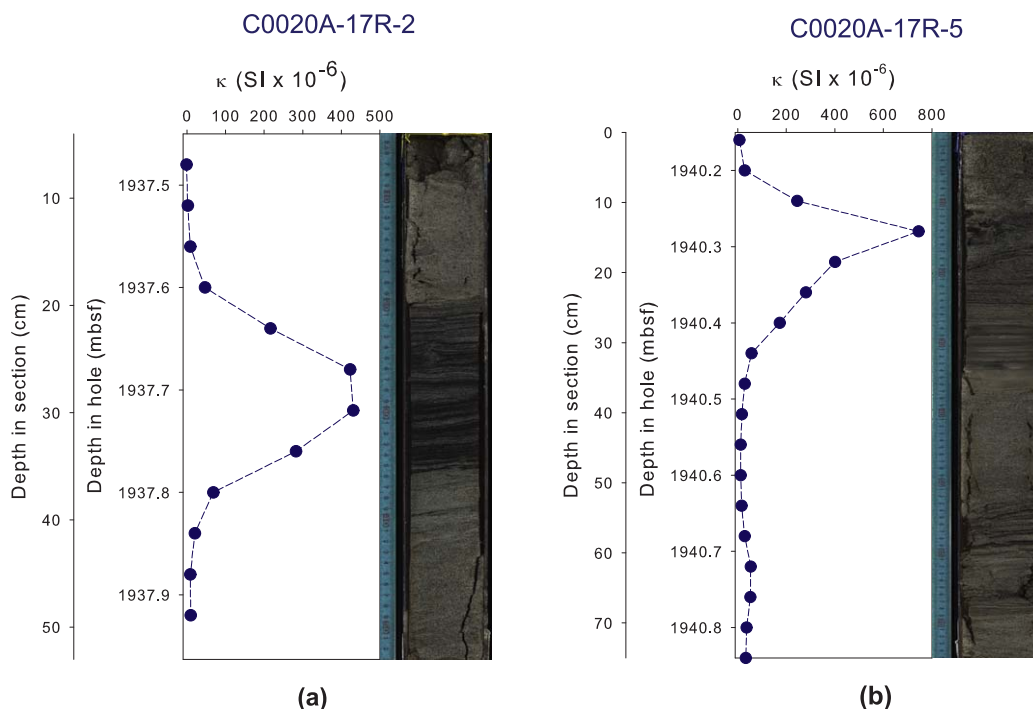


Figure 3. Shipboard measurements of magnetic susceptibility next to linescan core photos for two intervals within Unit III: (a) 1937.45–1937.95 mbsf in core 17R-2, (b) 1940.15–1940.84 mbsf in core 17R-5. These spikes in magnetic susceptibility occur in multiple lithologies but often occur within intervals containing organic-rich laminations. Typical background magnetic susceptibility throughout the hole is <100 ($\text{SI} \times 10^{-6}$).

-20°C . Six additional samples were sampled from archived sediment cores after Expedition 337. A 1 cm^3 subsample was cut from within each sample and measured for mass-specific magnetic susceptibility (χ , $\text{m}^3\text{ kg}^{-1}$), isothermal remanent magnetization (IRM) acquisition, and three-axis thermal demagnetization analysis. Semiconsolidated samples were wrapped in aluminum foil before IRM analysis to prevent loss of material during heating. In total, 144 discrete samples were analyzed for magnetic susceptibility and IRM analysis at the University of New Hampshire. To better constrain magnetic mineralogies, a subset of 10 samples that span a range of magnetic susceptibilities and represent all three cored lithostratigraphic units were further characterized at the Institute for Rock Magnetism, University of Minnesota. To constrain magnetic mineral compositions and grain size, diagnostic Curie temperature transitions at high temperature, the frequency dependence of magnetic susceptibility (χ_{fd} , %) and anhysteretic remanent magnetization (ARM, $\text{Am}^2\text{ kg}^{-1}$) were measured. In addition, three samples from high κ sandstones in Unit III were prepared as thin sections and analyzed with an electron microprobe at the University of Texas at Austin.

For sequential iron extraction analyses, sediment samples were taken after contamination screening from whole round cores designated for microbiology analyses [see also *Expedition 337 Scientists*, 2013; *Glombitza et al.*, 2016]. Sample splits were collected under anoxic conditions in a glove box, sealed in airtight bags under N_2 atmosphere, and stored (and shipped) frozen until further processing for geochemical analyses. A total of 47 samples were measured for total and extractable iron at the University of California at Riverside. Of these 47 samples, 41 were taken adjacent to whole round samples collected for magnetic analyses to allow for comparison of geochemical and magnetic records.

4.2. Magnetic Susceptibility

Magnetic susceptibility provides a general measure of the magnetic mineral concentration in sediments, regardless of grain size or composition. Here we report two variations of magnetic susceptibility. Both volume-specific and mass-specific magnetic susceptibility measurements were conducted using a Bartington MS2 magnetic susceptibility meter calibrated to water. Volume-specific susceptibility (κ) is reported from shipboard measurements conducted using a Bartington MS2C meter mounted on a *Geotek* whole round multisensor core logger. κ is a dimensionless ratio of an induced magnetization (M , here normalized

to volume in units of Am^{-1}) to the applied field (H , also in units of Am^{-1}) and is reported here in SI units. Mass-specific magnetic susceptibility (χ , $\text{m}^3 \text{kg}^{-1}$) is related to the volume susceptibility by the following expression: $\chi = \kappa/\rho$ where ρ is the density of the sample. χ was measured on all discrete core samples using a Bartington MS2B in low-frequency (LF) mode by recording the average of three measurements.

The frequency dependence of magnetic susceptibility (χ_{fd}) was determined for the subset of 10 samples that capture the range in magnetic susceptibility (both κ and χ). In-phase magnetic susceptibility was measured at low-frequency (465 Hz) and high-frequency (4650 Hz) susceptibility was measured in an alternating current field of 300 Am using a MAGNON variable frequency susceptibility meter at the Institute for Rock Magnetism. The reported χ_{fd} values are percentages, where $\chi_{fd} = [(\chi_{465\text{Hz}} - \chi_{4650\text{Hz}})/\chi_{465\text{Hz}}] \times 100$ [Deearing *et al.*, 1996].

4.3. Remanent Magnetization

Remanent magnetization is the relict magnetization of a material that exists in the absence of an applied field and reflects the sum of all magnetizations acquired over the history of the material. Remanent magnetization was measured in three positions using an HSM2 SQUID spinner magnetometer or a 2G 755 superconducting rock magnetometer at the UNH Paleomagnetism Laboratory. Prior to any manipulation of remanence with applied laboratory fields, each sample was measured for natural remanent magnetization (NRM), which represents permanent magnetization acquired by sediments during deposition in the Earth's magnetic field. Subsequently, samples were subjected to stepwise acquisition of IRM. IRM varies from NRM in that the magnetizing field is produced using laboratory instruments and is often much stronger (by orders of magnitude) than the Earth's magnetic field. IRM was imparted using an ASC IM-10 impulse magnetizer over sixteen steps from background to 1.1 T (see supporting information Table S1), and measured after each step. An induced magnetic field of 1.1 T is sufficient to approximately reach saturation IRM (SIRM) for lower coercivity minerals like magnetite, titanomagnetite, greigite, and pyrrhotite, but not for hematite or goethite. 1.1 T was sufficient to reach saturation in all samples from Hole C0020A. Coercivity was approximated from the IRM acquisition curves using a linear acquisition plot [Kruiver *et al.*, 2001] to obtain $B_{1/2}$, the field that imparts one-half of SIRM. A backfield IRM of -100 and -300 mT, in the opposite direction of the acquisition curve, were applied for the calculation of an S ratio (S_{100} and S_{300}) [e.g., Verosub and Roberts, 1995; Quinton *et al.*, 2011],

$$S_{xmT} = \frac{\text{IRM}_{-xmT}}{\text{SIRM}}$$

This approach allows for the determination of whether a magnetic assemblage is dominated by low coercivity (e.g., titanomagnetite and greigite) or high coercivity (e.g., goethite and hematite) minerals. Samples were not demagnetized prior to IRM acquisition; however, NRM is a small fraction of IRM in the vast majority of samples ($\sim 2\%$ in noncoal lithologies). Coal samples with low IRM were excluded from S-ratio and $B_{1/2}$ calculations. After acquisition of IRM at 1.1 T along a primary axis, fields of 400 and 120 mT were imparted at right angles to the primary axis [Lowrie, 1990]. We refer to IRM along the 1.1 T, 400 mT, and 120 mT axes as the hard, medium, and soft axes, respectively. Samples were then stepwise thermally demagnetized using an ASC TD48-SC magnetically shielded oven from room temperature to 680°C over 21 steps (see supporting information Table S2).

Measurements of anhysteretic remanent magnetization (ARM) were conducted on the same 10 samples measured for χ_{fd} , using a 2G Enterprises 760-R SQUID magnetometer with track system and inline ARM at the Institute for Rock Magnetism. ARM was acquired in a peak alternating field of 100 mT in the presence of a DC bias field of 0.05 mT. For these same 10 samples, an IRM of 100 mT was imparted using a pulse magnetizer and measured immediately afterward using the 2G magnetometer.

4.4. Curie Temperature Measurements

Different specimens from the same subset of 10 samples analyzed for ARM and χ_{fd} were measured for Curie temperatures using a high-temperature Geofyzika KLY-2 KappaBridge AC Susceptibility Bridge. For each sample, χ was monitored during heating from room temperature to 700°C and then back to 50°C . Replicates of each sample were run in either ambient atmosphere or under argon atmosphere.

4.5. Iron Speciation and Isotope Analyses

Samples from a range of lithologies across Units II, III, and IV were analyzed for sequentially extracted iron at the University of California, Riverside. To determine the fractions of amorphous Fe-(oxyhydr)oxides, crystalline Fe-oxides (e.g., hematite and goethite), and magnetite in the sediment a three-step chemical extraction method was applied, using ascorbate (Fe_{asc}), dithionite (Fe_{dith}), and oxalate (Fe_{oxa}), respectively [e.g., *Ferdelman*, 1988; *Kostka and Luther*, 1994; *Poulton and Canfield*, 2005; *Raiswell et al.*, 2010]. Each extraction step was carried out under anoxic conditions; frozen wet samples splits were taken in an anoxic (N_2) glove box. Each solution was deoxygenated with N_2 (for >30 min) prior to transfer into the glove box and subsequent addition to the sample. Extraction steps were performed in sequential order according to the following procedure: (1) ascorbate solution at pH 7.5 for 24 h, (2) dithionite at pH 4.8 for 2 h, and (3) oxalate a pH 3.2 for 6 h. Samples were agitated on a shaking table at room temperature during each extraction step. After centrifugation the supernatant was removed, and residues were washed with deoxygenated ultrapure water between each extraction step. The extracted iron from each phase was analyzed via a quadrupole inductively coupled plasma-mass spectrometer (ICP-MS; Agilent 7500c) upon dilution with 0.3M nitric acid, and reproducibility was monitored using an in-house mixed mineral standard. The reproducibility of this extraction method was determined to be better than 9%. To determine the water content, a separate fresh sample split was taken at the same time as the split for the Fe sequential extraction scheme and dried at 50°C. All Fe content data are reported on a dry sediment basis.

The highly reactive Fe pool in sediments (Fe_{HR}) is considered the part of Fe_T that is readily reactive with H_2S on timescales of 10^3 – 10^4 years. Fe_{HR} is operationally defined through carefully calibrated sequential extraction protocols [e.g., *Raiswell et al.*, 1994; *Kostka and Luther*, 1994; *Raiswell and Canfield*, 1998; *Poulton and Canfield*, 2005] and includes all three sequentially extracted Fe pools measured in this study as well as pyrite Fe (Fe_{py}). We calculated the Fe_{py} fraction by converting previously measured chromium-reducible sulfur (CRS) concentrations [*Glombitza et al.*, 2016] using pyrite stoichiometry FeS_2 . Standard ascorbate extraction has been shown to target amorphous Fe-(oxyhydr)oxides as well as less-crystalline Fe-carbonates [*Tessier et al.*, 1979; *Kostka and Luther*, 1994]. *Poulton and Canfield* [2005], however, have shown that a 24 h extraction at room temperature, as performed here, may be ineffective at extracting the crystalline forms of siderite and ankerite.

Total digestions for Fe (Fe_T) and Al were performed on approximately 100 mg of dry sediment applying a multiacid total digestion procedure (hydrofluoric acid, HF; hydrochloric acid, HCl; and nitric acid, HNO_3). Iron isotope compositions were determined on total iron and easily HCl-extractable iron phases. The latter were extracted using a cold 0.5 M HCl solution for 1 h (modified after *Kostka and Luther* [1994]), which leaches Fe from amorphous oxyhydr(oxides), ferrihydrite, Fe-monosulfides, Fe-carbonate, and some Fe from aluminosilicates (e.g., chlorite and glauconite), but not crystalline Fe-oxides or pyrite.

Sample solutions were purified for iron isotopes analysis following a standard anion-exchange chromatography method [e.g., *Severmann et al.*, 2006]. In brief, a sample aliquot from total digests or HCl extracts were transferred to 6 M HCl and loaded onto ~200 μl Bio-Rad AG1X8 anion exchange resin. The sample matrix was removed with a 5 ml 6 M HCl rinse. Iron was eluted with 2 ml 0.5 M HCl, evaporated and redigested by adding a few drops of concentrated HNO_3 . Purified Fe samples were measured via a multi collector-ICP-MS (MC-ICP-MS, ThermoScientific NeptunePlus) at Rutgers University. Samples were introduced into the MC-ICP-MS through an Apex desolvating nebulizer as 100 ppb solutions in 2% nitric acid and Fe isotopes were measured in medium resolution mode following the method of *Arnold et al.* [2004]. For correction of instrumental mass bias, a copper solution of known isotope composition (NIST-976 copper isotope standard) was added at the same concentration to the purified sample solution. In addition, the Fe isotope standard reference material IRMM-014 was measured before and after each two sample measurements. Precision and accuracy were monitored by measuring a geological standard reference material of known isotope composition (shale SDO-1, USGS), as well as a solution of IRMM-014 that had been spiked with purified ^{54}Fe isotope spike to lower its isotope composition by 1‰ [see *Arnold et al.*, 2004]. Fe isotope compositions are reported in standard delta notation ($\delta^{56}\text{Fe} = ([^{56}\text{Fe}/^{54}\text{Fe}_{\text{sample}}]/[^{56}\text{Fe}/^{54}\text{Fe}_{\text{standard}}] - 1) \times 1000$) relative to average igneous rock, which has an isotope composition of $\delta^{56}\text{Fe} = 0 \pm 0.05\text{‰}$ [*Beard et al.*, 2003]. The Fe isotope reference standard IRMM-014 has a $\delta^{56}\text{Fe}$ of -0.09‰ on this scale. The average external precision for replicate chemical processing and isotope analysis of five samples was 0.08‰ (2-SD) for $\delta^{56}\text{Fe}$. SDO-1 was measured as $0.06 \pm 0.12\text{‰}$ ($n = 5$) and ^{54}Fe -spiked IRMM-14 was measured as $1.04 \pm 0.10\text{‰}$ ($n = 13$).

4.6. Electron Microprobe Analysis

Three samples from 1937.655, 1941.085, and 1955.90 mbsf within high χ intervals in Unit III were prepared as thin sections and subjected to electron microprobe analysis (EMPA) for the elements Fe, Ti, Al, Mn, Cr, and S in an attempt to directly measure iron oxide or iron sulfide composition. EMPA measurements were performed using a JEOL 8200 Superprobe at the University of Texas at Austin Electron Microbeam Laboratory and calibrated with ilmenite, chromite, and celestite. Each of these samples was collected from high magnetic susceptibility intervals to maximize the likelihood of measuring an individual grain of titanomagnetite. EMPA was conducted using a 15 kV beam with a beam width of 5 μm . Results were generated as weight percent (wt %) oxide and converted to the percent of each element using the atomic weight of each element. Samples were first probed with energy-dispersive X-ray spectrometry (EDS) to view an approximate composition and then probed with the wavelength-dispersive X-ray spectrometry (WDS) for quantitative analysis.

5. Results

5.1. Magnetic Susceptibility

Laboratory χ closely matches the relative changes in the downcore record observed from the shipboard κ measurements suggesting little to no alteration of the magnetic mineral assemblage after core collection/sampling (Figure 4 and supporting information Table S3). The Pearson correlation coefficient between these two data sets is 0.93. LF χ ranges from -7.7 to $265.6 \times 10^{-8} \text{ kg/m}^3$ (mean: $18.3 \times 10^{-8} \text{ kg/m}^3$, median: $9.0 \times 10^{-8} \text{ kg/m}^3$). χ_{fd} ranges from 2.2 to 12.3%, and notably increases in samples with higher χ (Figure 4). Measurements of χ_{fd} in high χ samples of Unit III approach the theoretical maximum for ferrimagnetic materials ($\sim 15\%$) [Dearing *et al.*, 1996].

5.2. IRM Acquisition and Backfield IRM

All samples show acquisition curves typical of low-coercivity minerals reaching SIRM below 200 mT (Figure 5). Likewise, the soft axis (120 mT) contains the dominant fraction of IRM after three-axis magnetization. $B_{1/2}$ ranges between 23 and 98 mT (mean: 48 mT), with the highest coercivities in Unit II at approximately 1500 mbsf and decreasing in Unit III (Figure 6). S_{300} varies from 0.76 to 1.04 with a mean of 0.92. S_{100} and S_{300} are lower in Units II and IV compared to Unit III (Figure 6).

NRM intensity follows trends in magnetic susceptibility ranging from 0.3 to 68,600 mA/m (median: 12 mA/m) (Figure 6). Similarly, SIRM follows a pattern similar to χ and ranges from 31 to 221,100 mA/m (median: 1262 mA/m). SIRM/ χ ratios are elevated in a substantial portion of samples in Unit II, and several samples in Units III and IV (Figure 6).

5.3. Thermal Demagnetization

Thermal demagnetization removed all IRM by 580°C or below in all samples, and in all samples the primary carrier of IRM was the Z (soft) axis throughout demagnetization. Demagnetization curves in samples from Unit II, Unit III between 1920–1925 and 1995–2002 mbsf, and in Unit IV are characterized by a linear decrease to 580°C (Figure 5a). Samples between 1925 and 1973 mbsf have demagnetization curves in which soft IRM decreases overall to 580°C but with a pronounced decrease between 275 and 350°C (Figures 5b and 5c). In the interval 1979–1993 mbsf, demagnetization curves decrease linearly from room temperature to 350–400°C (Figure 5d). The fraction of soft IRM lost between 0 and 350°C and 275 and 350°C increases in Unit III. There is a pronounced increase in the fraction of soft IRM lost below 350–400°C at depths between 1925 and 1973 mbsf (Figures 6 and 7 and supporting information Figure S1). Between 1979 and 1993 mbsf, and at 1826, 2110, 2307, 2309, and 2463 mbsf, there is an enhanced fraction of soft IRM lost between 0 and 350°C but no distinct drop at 275°C. The shift in unblocking temperature is observed in all siliciclastic lithologies in the coal-bearing unit, and not driven by changes in depositional environment.

5.4. Anhysteretic Remanent Magnetization

Ten samples measured for ARM range from 8.6×10^{-6} to $1.07 \times 10^{-3} \text{ Am}^2/\text{kg}$. The highest ARM values are in Unit III (average: $3.8 \times 10^{-4} \text{ Am}^2/\text{kg}$) compared to Units II and IV (average: $5.5 \times 10^{-5} \text{ Am}^2/\text{kg}$) (Figure 6 and supporting information Figure S1 and Table S4). ARM/IRM ratios are relatively consistent throughout the record (0.01–0.11) with one high value in Unit III (0.58).

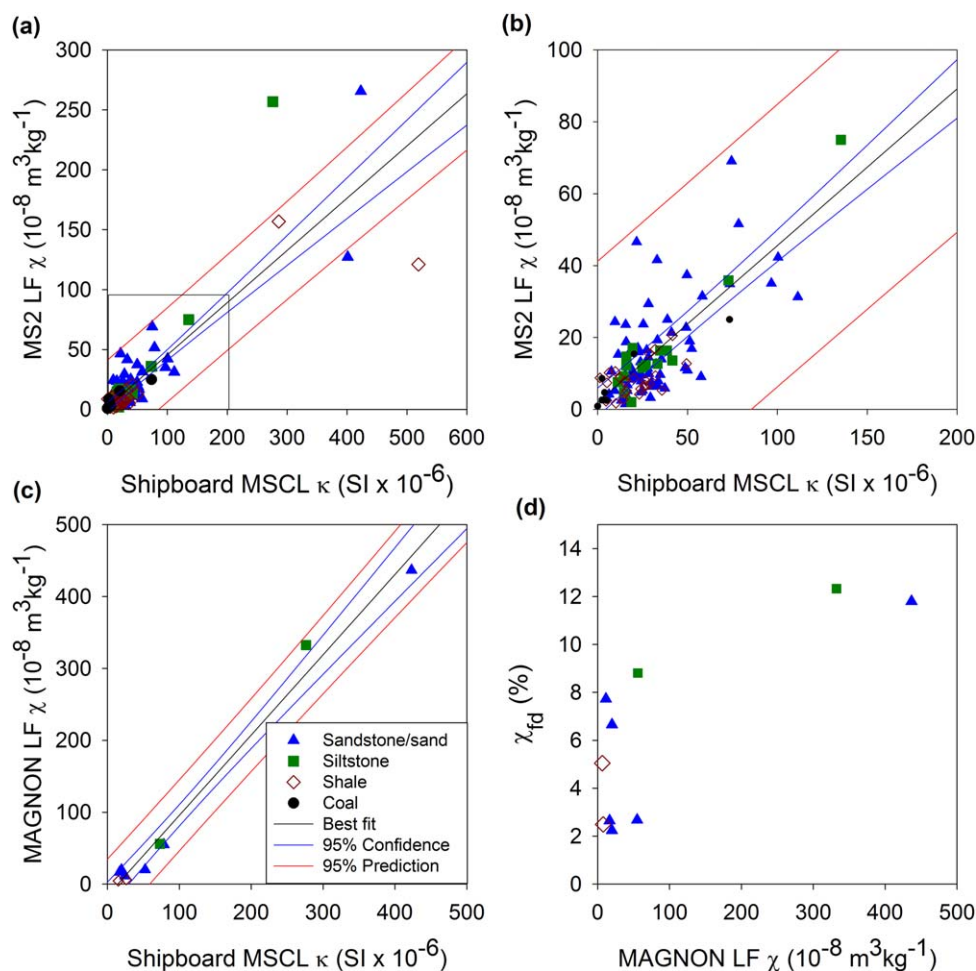


Figure 4. (a) Correlation of shipboard volume-specific magnetic susceptibility (κ) from multisensor core logging (MSCL) and postcruise MS2 mass-specific low-frequency magnetic susceptibility measurements (χ). Correlation between data indicates little to no alteration to the magnetic mineral assemblage since sampling. (b) Zoomed-in view of the lower magnetic susceptibility samples. (c) Correlation of shipboard and postcruise MAGNON measurements. (d) Relationship of χ_{fd} to χ . Frequency dependence increases in the high magnetic susceptibility samples of Unit III.

5.5. Curie Temperature Measurements

All measurements for Curie temperature show an increase in χ when heated above 300°C and then a rapid removal of χ below 600°C (supporting information Figure S2 and Table S5). The increase in χ is observed in samples both under open atmosphere and argon, but in some cases is reduced under argon. The increase in χ is generally most pronounced in samples from Unit III and IV.

5.6. Iron Speciation and Isotope Compositions

Total Fe concentrations were lowest, and variability highest, in the coal bearing Unit III (average Fe_T 2.3 ± 1.5 wt %, Figures 6 and 7 supporting information Table S6). The low concentrations and high variability of Fe are also reflected in the Fe_T/Al ratios (average Fe_T/Al 0.3 ± 0.16) in this unit. In Units II and IV, concentrations are in the range typical for continental margin sediments (average Fe_T 3.5 ± 0.8 wt %) with Fe_T/Al ratios (0.41 ± 0.08) closely resembling that of average continental crust (0.44) [Taylor and McLennan, 1985]. Low Fe_T and Fe_T/Al in Unit III coincide with low sulfur concentrations [Glombitza et al., 2016] and low Fe_{HR} concentrations.

Fe_{asc} is largely absent throughout all three units (supporting information Table S6 and Figure S3) with concentrations below detection limit (2 mg/kg) except for two samples that are <50 mg/kg. Previous mineralogical investigations of sediments from Unit III and Unit IV have shown the presence of siderite, which was

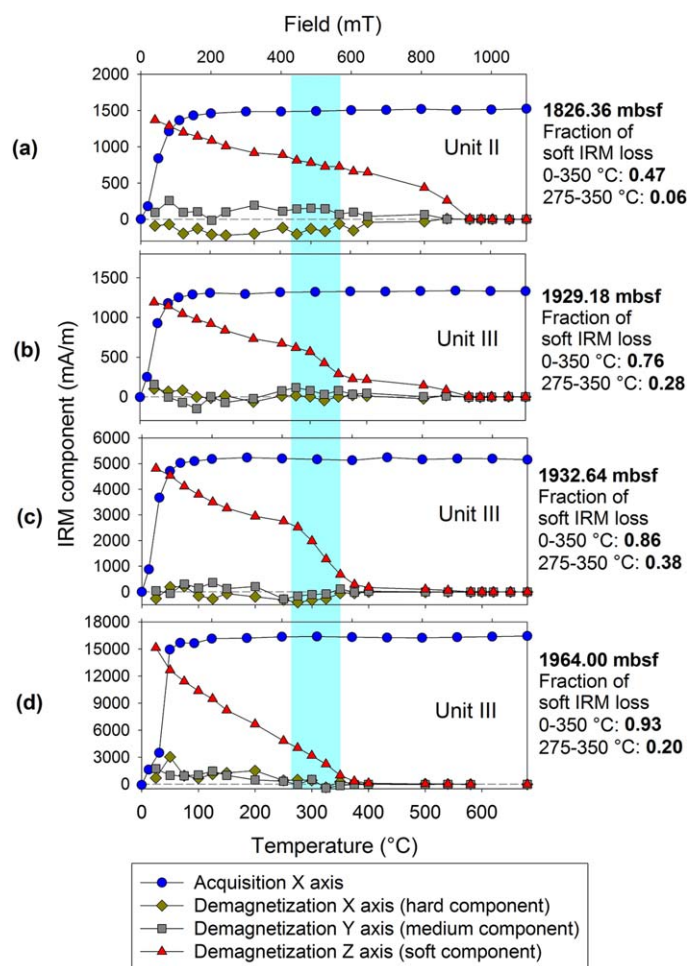


Figure 5. Example IRM and thermal demagnetization results showing increase in the fraction of IRM loss between 275 and 350°C (blue band) in the coal-bearing part of Unit III. All samples show low-coercivity and saturation by 200 mT. (a) Samples in Units II, IV, and the upper portion of Unit III away from the coals show a relatively linear decrease in IRM to 580°C. (b–d) Within Unit III near the coals (between 1930 and 1995 mbsf) the fraction of IRM lost between 275 and 350°C increases. The shift in unblocking temperature is observed in all siliciclastic lithologies in the coal-bearing unit, and not driven by changes in depositional environment.

III, in contrast, Fe_{Oxa} reached maximum concentrations of up to 1.36 wt %, comprising up to 95% of the Fe_{HR} pool. Coal-bearing Unit III had the lowest Fe_{py} concentrations (average 0.1 wt %) and relative proportion (average 35% of Fe_{HR}). Fe_{py} concentrations and relative proportion were highest in Unit II, where it was the dominant fraction of Fe_{HR} in 6 out of 11 samples. In Unit IV, Fe_{Oxa} was on average the dominant fraction although for one sample Fe_{py} made up 90% of Fe_{HR} .

Iron isotope compositions were only measured in samples from Unit III. The cold 0.5M HCl leach was used as an approximation to measure the isotope composition of the reactive Fe pool ($Fe_{0.5M\ HCl}$). Although previous calibrations of the HCl extractions have been shown to be ineffective in leaching Fe from pyrite or magnetite, $Fe_{0.5M\ HCl}$ concentrations exceeded Fe_{HR} concentrations in all samples, confirming that $Fe_{0.5M\ HCl}$ includes significant amounts of Fe from aluminosilicates such as chlorite and glauconite. Iron isotope compositions for coal beds in Unit III (total organic carbon or TOC > 40 wt %) were clearly elevated in both Fe_T and $Fe_{0.5M\ HCl}$ fractions with $\delta^{56}Fe_T$ of $+0.99 \pm 0.74\text{‰}$ and $\delta^{56}Fe_{0.5M\ HCl}$ of $+0.71 \pm 0.79\text{‰}$. Iron isotope compositions in the remaining samples from Unit III were less variable and $\delta^{56}Fe$ values of $+0.07 \pm 0.14\text{‰}$ for Fe_T and $-0.14 \pm 0.26\text{‰}$ for $Fe_{0.5M\ HCl}$, which is closer to the isotope composition of average igneous rocks.

not revealed specifically by our extraction technique, but was likely extracted along with magnetite in the oxalate extraction, with less crystalline forms extracted during the dithionite extraction. This discrepancy suggests that our Fe_{asc} leach did not extract the Fe-carbonates present in these two units, and we therefore assume that any crystalline siderite was primarily extracted during the oxalate treatment. Further, given the age of the sediments (>20 Ma) any amorphous or more labile Fe would have undergone reduction or been converted to more crystalline Fe oxides. The dithionite treatment, which specifically targets crystalline Fe oxides such as lepidocrocite, goethite, and hematite, recovered only little Fe_{dith} (0.03 ± 0.03 wt %) in all three units (supporting information Table S6 and Figure S3). In Units II and IV Fe_{dith} made up on average 4.4% of the Fe_{HR} pool, whereas in Unit III the relative proportion of Fe_{dith} in the Fe_{HR} pool reached up to 30% despite the absolute concentrations remaining low.

Consistent with rock magnetic data, significant magnetite (extracted as Fe_{Oxa}) was present in most layers sampled (Figures 6 and 7 supporting information Figure S3). An exception was three samples near the top of Unit III where Fe_{Oxa} was ≤ 0.01 wt %. Near the base of Unit

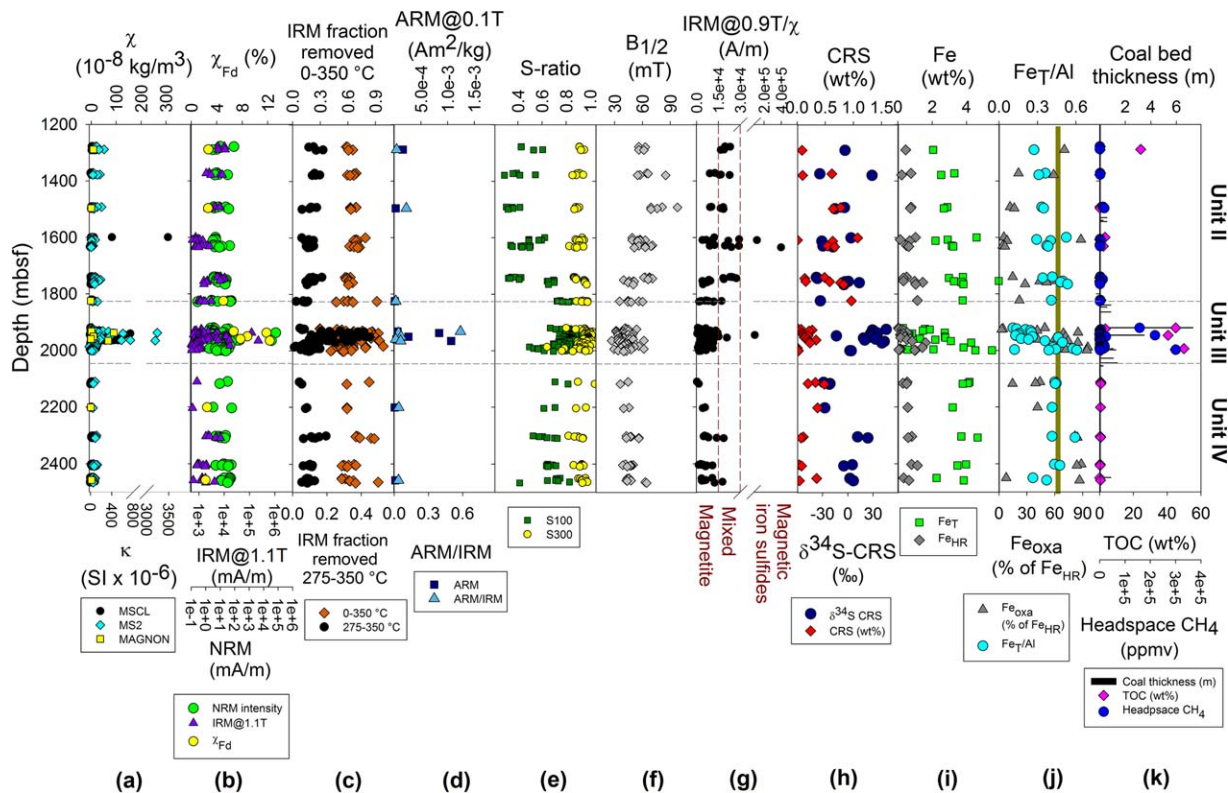


Figure 6. Key down core rock magnetic and geochemical results. (a) Magnetic susceptibility, (b) frequency dependence of magnetic susceptibility, isothermal remanent magnetization (IRM) at 1.1 T, and natural remanent magnetization (c) fraction of soft isothermal remanent magnetization (IRM) removed during thermal demagnetization (0–350 and 275–350°C), (d) anhysteretic remanent magnetization (ARM) and ARM/IRM ratios, (e) –100 and –300 mT S-ratios (f) coercivity ($B_{1/2}$), (g) IRM at 0.9T/ χ , range of magnetite, magnetitic iron sulfides, and mixed magnetite and magnetic iron sulfides from *Larrasoana et al.* [2006]. Chromium-reducible sulfur (CRS) [*Glombitza et al.*, 2016], (h) $\delta^{34}\text{S}$ of the CRS fraction [*Glombitza et al.*, 2016], (i) highly reactive (Fe_{HR}) and total (Fe_{T}) iron, (j) Fe/Al ratios (vertical green bar represents average continental Fe/Al) (0.44) [*Taylor and McLennan*, 1985] and oxalate-extractable iron as a fraction of Fe_{HR} (i) coal-bed thickness [*Expedition 337 Scientists*, 2013], and (k) total organic carbon (TOC) and headspace methane [*Expedition 337 Scientists*, 2013].

5.7. Electron Microprobe Analysis

Within the three high magnetic susceptibility sand/sandstone samples collected from Unit III for EMPA, all opaque/high backscatter minerals analyzed with EDS showed peaks that were suggestive of ilmenite, pyrite, rutile, apatite, or siderite. Very few grains showed EDS peaks suggestive of magnetite, and these were generally in grains that were too small for analysis. WDS analysis of grains large enough for analysis confirmed the dominant presence of ilmenite and pyrite, with minor rutile (supporting information Table S7). All grains that were suspected to be (titano)magnetite were less than 5 μm and produced poor WDS results (40–60 wt % total elemental content) that contained considerable Si and Al content suggesting the beam overlapped from high-backscatter potential iron oxide grains to the surrounding low-backscatter grains of quartz and clays due to the small grain size of the target grains.

6. Discussion

6.1. Magnetic Mineral Assemblage

Results of IRM acquisition (low-coercivity) and unblocking temperatures (580°C) suggest a magnetic mineral assemblage dominated by detrital magnetite for most samples in Unit II and Unit IV. Our measurements show little evidence for contribution from hematite, goethite, greigite, or pyrrhotite to the magnetic mineral assemblage. All samples at Site C0020A saturated below 200 mT suggesting low-coercivity minerals dominate the magnetic properties reported here. Plots of SIRM/χ and $B_{1/2}$ are consistent with titanomagnetite for all samples but three (Figure 8). Two samples in Unit II and one sample in Unit III show high SIRM/χ ratios typical of magnetic iron sulfides [*Dekkers*, 1988; *Roberts*, 1995; *Dekkers et al.*, 2000]. However, these samples do not show a characteristic unblocking temperature for greigite or pyrrhotite [*Lowrie*, 1990; *Roberts*, 1995]. These samples possibly represent a minor component of authigenic mineral formation associated with

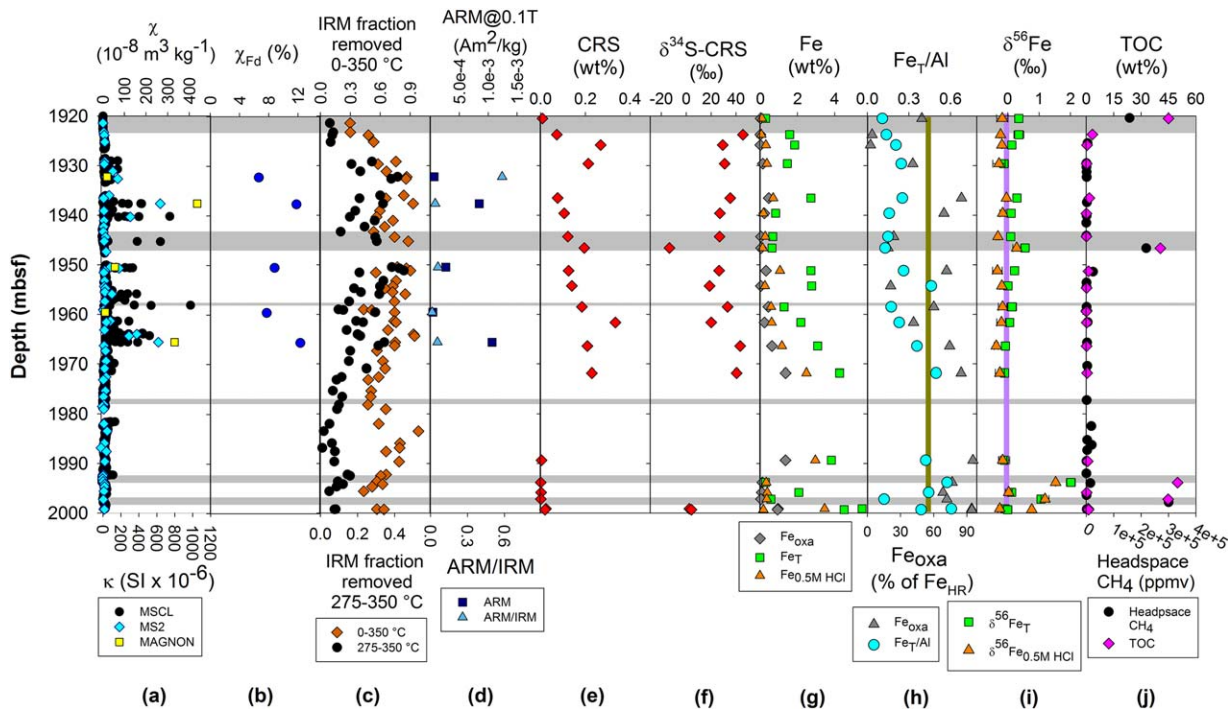


Figure 7. Detailed view of down core rock magnetic and geochemical results for the key coal-bearing interval of record shown in Figure 6. (a) Magnetic susceptibility, (b) frequency dependence of magnetic susceptibility, (c) fraction of soft IRM removed during thermal demagnetization (0–350 and 275–350°C), (d) ARM and ARM/IRM ratios, (e) chromium-reducible sulfur (CRS) [Glombitza et al., 2016], (f) $\delta^{34}\text{S}$ of the CRS fraction [Glombitza et al., 2016], (g) highly reactive (Fe_{HR}), HCl-extractable (Fe_{HCl}) and total (Fe_{T}) iron, (h) Fe/Al ratios (vertical green bar represents average continental Fe/Al) [Taylor and McLennan, 1985] and oxalate-extractable iron as a fraction of Fe_{HR} , (i) $\delta^{56}\text{Fe}$ of total ($\delta^{56}\text{Fe}_{\text{T}}$) and HCl-extractable ($\delta^{56}\text{Fe}_{\text{HCl}}$) iron, vertical purple bar represents average igneous $\delta^{56}\text{Fe}$ from Beard et al. [2003], and (j) total organic carbon (TOC) and headspace methane [Expedition 337 Scientists, 2013]. Shaded horizontal bars indicate coal intervals.

diagenesis of marine sediments [Larrasoña et al., 2007] or rapid burial of detrital pyrrhotite [Hornig and Roberts, 2006].

Samples in Unit III that show a significant portion of soft IRM with an unblocking temperature at approximately 350°C are consistent with the demagnetization of magnetic iron sulfides, maghemite, or (titano)-magnetite (either fine-grained magnetite or TM30 titanomagnetite). However, a few samples have SIRM/ χ and $B_{1/2}$ that are consistent with at least a partial greigite or pyrrhotite component [Peters and Dekkers, 2003] but do not correspond to samples with a 350°C unblocking temperature. Additional measurements of χ after long exposure to oxygen (approximately 2 years) do not show a decrease relative to the shipboard

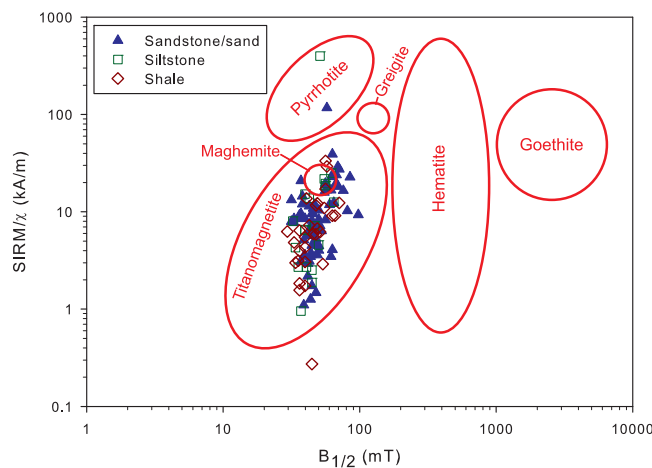


Figure 8. Crossplot of SIRM/ χ and $B_{1/2}$ for all samples from Units II, III, and IV. Mineral ranges from Peters and Dekkers [2003].

measurements, indicating that authigenic magnetic iron sulfides vulnerable to oxidation are not likely a significant component. A magnetic mineral assemblage with a large, metastable magnetic iron sulfide component would likely experience a loss in χ after prolonged exposure to oxygen [Hunger and Benning, 2007]. EMPA analysis indicated that iron sulfides present in Unit III are dominantly pyrite, which generally is characterized by very low magnetic susceptibility [Waters et al., 2008].

IRM acquisition and χ results are consistent with the dominant presence of magnetite but a possible minor maghemite ($\gamma\text{-Fe}_2\text{O}_3$) component cannot be ruled out. Maghemitization of

titanomagnetite can occur in oxygenated sediments, but is a more common component in pelagic settings where low sedimentation rates yield long exposure times to oxygenated bottom waters [Smirnov and Tarduno, 2000; Xu et al., 1997]. In this record, sediments from nonwetland environments were likely exposed to oxygenated bottom waters, but due to high sedimentation rates (~ 100 m/Ma over the entire hole) [Phillips et al., 2016] and high TOC throughout Site C0020 (up to 50 wt % in coal layers) [Expedition 337 Scientists, 2013], magnetite, probably of detrital origin, was likely buried quickly into anoxic conditions.

In our record, magnetite is the mineral most likely associated with the ~ 300 – 400°C unblocking temperature, due to its decreased grain size compared to the background coarser-grained magnetite with an unblocking temperature of $\sim 580^\circ\text{C}$, close to the Curie temperature. The unblocking temperature of magnetite can deviate from the Curie temperature decreasing below 575°C in cases where the particle size is less than 50 nm [Dunlop, 1973a; Winklhofer et al., 1997]. Our Curie temperature measurements show an increase in χ due to alteration at 300 – 350°C and a rapid decrease below 600°C . Our results show a consistent behavior in Curie temperature measurements in both types of samples with unblocking temperatures of 580 and 300 – 400°C . In Unit III, between 1925 and 1975 mbsf demagnetization curves suggest that there is a mix of detrital and authigenic magnetite, while between 1975 and 2000 mbsf the magnetic mineral assemblage may be dominated by authigenic magnetite. Increased ARM in Unit III (Figure 6) also suggests fine-grained magnetite is present. Increased χ_{fd} in Unit III indicates the increased presence of superparamagnetic magnetite at room temperature suggesting magnetite grains < 30 nm [Dunlop, 1973b]. In summary, rock magnetic measurements suggest detrital magnetite composes the primary magnetic mineral assemblage throughout C0020A with an additional fine-grained secondary phase (authigenic) of magnetite with lower unblocking temperatures within Unit III.

6.2. Depositional Environment

In our data set, there is no clear change in magnetic mineralogy or magnetic susceptibility that is associated with a particular major change in lithology (supporting information Figure S4). Sandstone/sand samples have an average χ of $18.9 \times 10^{-8} \text{ m}^3 \text{ kg}^{-1}$, siltstone $26.8 \times 10^{-8} \text{ m}^3 \text{ kg}^{-1}$, and shale $15.7 \times 10^{-8} \text{ m}^3 \text{ kg}^{-1}$. The ultimate source for detrital magnetite at Site C0020A is most likely from weathering of rocks within northern Honshu. Subangular fragments were commonly observed within Unit III [Expedition 337 Scientists, 2013] indicating minimal transport from source to deposition. Titanomagnetite is a common constituent in volcanic rocks [Akimoto and Katsura, 1959; Sakuyama and Nesbitt, 1986; Hoshi and Teranishi, 2007; Ohba et al., 2007; Suzuki, 2008], magnetite-series granitic rocks [Takagi, 2004], and hornfels facies metamorphic rocks [Tsusue, 1962] from Honshu. Magnetite has also been observed as the primary detrital magnetic mineral in the Nankai accretionary complex [Kanamatsu et al., 2012; Zhao et al., 2013; Kars and Kodama, 2015] and Japan Sea [Razjigaeva and Naumova, 1992; Vigliotti, 1997]. Paleomagnetic studies of sediments from DSDP and ODP sites in the Japan Trench and fore-arc basin show stable magnetic remanance [Hall and Smeltzer, 1980; Niitsuma, 1986; Kanamatsu and Niitsuma, 2004], but do not directly address magnetic mineral assemblage. The titanomagnetite-dominant magnetic mineral assemblage at C0020A is consistent with sites and lithologic sources around the Japanese margin.

Magnetite has a density (5.20 g/cm^3) nearly double that of quartz (2.65 g/cm^3) [Schön, 2004], and commonly shows hydraulic sorting in beach and fluvial environments [e.g., Slingerland and Smith, 1986; Komar, 1989]. The anomalous increases in χ (to ~ 100 – $400 \times 10^{-8} \text{ kg/m}^3$) are similar to the range observed in modern titanomagnetite placer deposits (~ 50 – $2000 \times 10^{-8} \text{ kg/m}^3$) [Badesab et al., 2012]. However, the presence of fine-grained SP magnetite and the fact that increases in χ also occur in fine-grained rocks at Site C0020 suggest placer sorting is not the cause of the observed increases in χ .

The increases in magnetic susceptibility within Unit III are likely a result of additional authigenic precipitation of magnetite rather than a rapid additional influx of detrital magnetite. Given the high sedimentation rate of site C0020, cm-scale intervals of high magnetic susceptibility likely do not correspond to changes in provenance. These cm-scale increases in magnetic susceptibility occur in multiple lithologies: sand, siltstone, and shale, but only in the coal-bearing unit and often associated with organic-rich laminations. In addition, the high χ samples correspond to increased χ_{fd} suggesting an increase of superparamagnetic fine-grained material within high χ intervals.

6.3. Biogeochemical Implications

We suggest that in the terrestrial/estuarine sediments of Unit III, the presence of ultrafine magnetite resulting in lower unblocking temperatures, increased ARM, and increased χ_{fd} is the result of authigenic magnetite formation during early burial. Iron reduction of Fe(III) present in amorphous iron oxides under anoxic conditions can result in the extracellular production of ultrafine-grained magnetite [Lovley *et al.*, 1987]. In addition, magnetosome formation by magnetotactic bacteria can also be a biogenic source of fine-grained magnetite [e.g., Blakemore, 1982; Kirschvink and Chang, 1984; Bazylinski *et al.*, 1988; Devouard *et al.*, 1988; Bazylinski and Frankel, 2004]. Experimental investigations of magnetosomes in magnetotactic bacteria have shown that there is no detectable Fe isotope fractionation in intracellular magnetite [Mandernack *et al.*, 1999]. The heavy $\delta^{56}\text{Fe}_T$ values in Unit III therefore suggest that the fine-grained authigenic magnetite was formed dominantly extracellularly as a by-product of dissimilatory Fe reduction.

Magnetic properties further support a dominantly extracellular origin of magnetite in the coal-bearing Unit III. While magnetotactic bacteria typically produce magnetite within the single-domain range, iron reducers like *Geobacter metallireducens* facilitate the production of both single-domain- and superparamagnetic-sized magnetites [Moskowitz *et al.*, 1989, 1993]. Multiyear experiments demonstrate that Fe-reducing bacteria can produce superparamagnetic to multidomain-sized magnetite [Abrajevitch *et al.*, 2016]. Intervals of high χ in Unit III are often associated with laminated sediments, suggesting benthic anoxia at the time of deposition, which would favor anoxic extracellular production rather than magnetotactic production at the nitrogenous to ferruginous transition. Extracellular production of magnetite under anoxic conditions by *G. metallireducens* can produce higher magnetite output per biomass compared to magnetotactic bacteria [Lovley, 1991a, 1991b]. High χ_{fd} values in Unit III indicate a greater abundance of superparamagnetic magnetite, which in turn suggests the presence of extracellular magnetite. In either case, iron reduction plays an important role, either by directly contributing to magnetite formation or by supplying Fe(II) that diffuses to the nitrogenous-ferruginous transition zone [e.g., Froelich *et al.*, 1979; Canfield and Thamdrup, 2009; Roberts, 2015].

Precipitation of authigenic magnetite due to degradation of hydrocarbons has been widely observed [e.g., McCabe *et al.*, 1987; Elmore and Crawford, 1990; Elmore *et al.*, 1997] and can result in increases in magnetic susceptibility [e.g., Saunders *et al.*, 1991; Hall and Evans, 1995; Mewafy *et al.*, 2011; Atekwana *et al.*, 2014; Pérez-Pérez *et al.*, 2016]. In a similar process, we suggest that coal deposits can promote the authigenic precipitation of magnetite. As we discuss below, the depositional/diagenetic setting and previously observed microbial communities suggest that iron reduction has played a major role within Unit III and contributed to authigenic magnetite formation.

6.3.1. Iron Reduction and Sulfur Limitation

The depositional environment along with associated geochemical and microbiological characterization suggests Unit III is an interval that is able to host iron-reducing bacteria during burial. Iron is the most abundant electron acceptor in freshwater settings [Nealson and Saffarini, 1994]. Phylogenetic analysis of 16S rRNA indicates an increased presence of Firmicutes and Proteobacteria phylum bacteria within Units III and IV [Inagaki *et al.*, 2015], a phylum that includes iron-reducing bacteria [Li *et al.*, 2011; Hori *et al.*, 2015]. The low-sulfur terrestrial/estuarine environment of Unit III [Expedition 337 Scientists, 2013] and terrestrial microbial communities within this unit [Inagaki *et al.*, 2015] suggest a limited role for sulfate reduction, thus alteration of magnetic minerals is not likely affected by reaction with hydrogen sulfide. Although some sulfur is present within this interval and pyrite was observed, CRS decreases within Unit III relative to Units II and IV (Figure 6) [Glombitza *et al.*, 2016]. The decrease in CRS concentrations suggests low sulfate reduction rates and muted iron sulfide precipitation, consistent with limited sulfate availability within a brackish-to-freshwater environment. Highly enriched $\delta^{34}\text{S}$ of CRS in Unit III (median: +26.9‰, maximum: +45.6‰) further indicates an increasingly smaller and therefore ^{34}S -enriched sulfate reservoir, where sulfate reduction was fueled by sulfate that was regenerated in a cryptic sulfur cycle [Glombitza *et al.*, 2016] (Figures 6 and 7). Under sulfate-limiting conditions, and in the presence of Fe(III) from Fe-oxides or glauconite, sulfide may be partially reoxidized to sulfate to maintain slow sulfate-reducing metabolism that does not generate substantial sulfide minerals.

The common occurrence of authigenic siderite nodules throughout Units III and IV [Expedition 337 Scientists, 2013] also indicates a diagenetic environment where microbial Fe reduction was a significant metabolic pathway during organic carbon burial. Substantial alteration during the heating step for Curie temperature

measurements of Unit III sediments (supporting information Figure S2) is consistent with alteration of siderite to magnetite and maghemite during heating [Pan *et al.*, 1999, 2000, 2002]. Laboratory experiments and equilibrium calculations by Bell *et al.* [1987] suggest that magnetite formation is favored under more alkaline conditions, siderite formation is favored under more acidic conditions, and both magnetite and siderite would be present at pH 7.0 if H₂S is not present. The upward transition from a neutral-to-acidic, freshwater environment to alkaline, brackish environment in Unit III [Gross *et al.*, 2015] are consistent with our observations of authigenic magnetite that overly and overlap with the abundant siderite nodules in the base of Unit III and in Unit IV [Expedition 337 Scientists, 337]. The Fe(II) produced via iron reduction is available to react with bicarbonate within the methanic zone when H₂S is not present [Berner, 1981; Maynard, 1982; Postma, 1982] or in an environment in which rates of iron reduction are greater than sulfate reduction [Pye *et al.*, 1990]. Fe(III)-reducing bacteria can produce microbially derived siderite as a direct by-product of dissimilatory iron reduction [Lovley and Phillips, 1986; Mortimer and Coleman, 1997]. The decrease in CRS within siliciclastic sediments of Unit III [Expedition 337 Scientists, 2013; Glombitza *et al.*, 2016] indicates sulfur limitation and an environment in which the sink for Fe(II) produced during iron reduction are siderite or magnetite rather than pyrite. Overall, geochemical and mineralogical observations from Site C0020 suggest that the terrestrial to marine transition Unit III provided a diagenetic environment favorable for microbial magnetite formation.

Magnetite is typically low or absent in anoxic coastal margin sediments for two reasons: (1) In marine sediments where sulfate concentrations are relatively high, bacterial sulfate reduction usually dominates over microbial Fe reduction, suppressing authigenic magnetite formation. (2) Magnetite of detrital origin dissolves during burial in the presence of H₂S [e.g., Canfield and Berner, 1987; Karlin, 1990]. A slight decrease in S₁₀₀ and increase in B_{1/2} in the marine Unit II relative to Units III and IV (Figures 6e and 6f) may indicate any minor presence of high coercivity minerals resistant to H₂S dissolution (hematite and goethite) become more concentrated in sulfidic sediments as low coercivity magnetite is preferentially removed [e.g., Garming *et al.*, 2005]. With increasing burial depth magnetite and other crystalline Fe oxides are replaced by pyrite or its precursor greigite. Previous studies have shown that greigite formed during sulfidization may contribute to late stage remanence acquisition long after the original deposition [Rowan and Roberts, 2006]; however, we found little evidence for the presence of greigite. IRM@0.9/χ values possibly suggestive of a minor presence of magnetic iron sulfides are largely restricted to Unit II (Figure 6g). Magnetite concentrations of up to 1.36 wt % in Unit III suggest that either magnetite has been added or that detrital magnetite has escaped sulfidization during burial diagenesis.

Collectively the rock magnetic, Fe isotope, and Fe speciation data suggest that the coal-bearing Unit III has undergone postdepositional diagenetic alteration that has led to the removal or replacement of the original mineral assemblage. Fe_T and Fe_{HR} are markedly decreased in Unit III, but the large variability in Fe_T/AI ranging between 0.11 and 0.61 in this unit suggests that Fe has been removed from some intervals, and added to others, during burial diagenesis. Bulk Fe isotope data are consistent with this interpretation: a shift in δ⁵⁶Fe_T cannot be achieved by internal redistribution of reactive Fe into different minerals during early diagenesis. Elevated δ⁵⁶Fe_T values of up to 2‰ can only be achieved through significant loss of light Fe or addition of heavy Fe. All except one sample with δ⁵⁶Fe_T > 0.3‰ are associated with Fe_T/AI values that are significantly below the detrital baseline (supporting information Figure S5), suggesting that loss of Fe_{HR} was the primary control on bulk Fe isotope compositions. The Fe isotope compositions for the 0.5M HCl extractions show a trend very similar to the bulk isotope values (Figure 7). The slightly lower δ⁵⁶Fe_{0.5M HCl} values, closer to the detrital baseline, confirm that this extraction likely included significant Fe from silicates while at the same time being ineffective at dissolving other phases of the Fe_{HR} pool that may have a heavier isotope composition. The increase in δ⁵⁶Fe_T at the base of Unit III corresponds to a shift from a mixed detrital and authigenic magnetite (a pronounced drop in soft IRM from 275 to 350°C superimposed on a slower drop from 0 to 575°C) to mostly authigenic magnetite (linear decrease in soft IRM from 0 to 350°C). Where authigenic magnetite composes a higher fraction of total magnetite, the near-zero δ⁵⁶Fe values from igneous magnetite contribute less to masking the heavy δ⁵⁶Fe composition of authigenic magnetite.

Vertical fluid advection, such as during groundwater fluid flow, has been shown to alter the remanent magnetization [Rowan and Roberts, 2006] as well as the Fe isotope composition [Rouxel *et al.*, 2008] of the original mineral assemblage. Low-salinity groundwater may stimulate microbial Fe-oxide reduction as well as oxidative precipitation of Fe-oxides. The low CRS concentrations in Unit III suggest the lack of pyrite

precipitation and/or the removal of pyrite through oxidation that could occur through alteration by groundwater. Magnetite that is produced during microbial Fe reduction typically has a heavy isotope composition [Johnson *et al.*, 2005], while the pore water Fe(II) that is being generated during redox recycling will be isotopically light [Severmann *et al.*, 2006]. Rouxel *et al.* [2008] have observed a wide range (−2 to +1.5‰) in the Fe_{HR} isotope composition of sediments that have been affected by groundwater alteration in a subterranean estuary. Although the sediments in Unit III only show near-detrital or positive $\delta^{56}\text{Fe}_{\text{T}}$ values it is likely that alteration was caused by a similar combination of processes. These processes may include dissolution of the original mineral assemblage, conversion of Fe-oxide to authigenic magnetite and potentially also formation of new authigenic mineral phases such as glauconite and siderite. We propose that the combined effect of these processes was the observed decrease in Fe_{T} and Fe_{HR} , variable $\text{Fe}_{\text{T}}/\text{Al}$, ratios and heavy Fe_{T} and $\text{Fe}_{0.5\text{M HCl}}$ isotope compositions.

6.3.2. Peat/Lignite As Source of Electron Donors

The presence of fine-grained biogenic magnetite occurs over a broad interval containing numerous coal beds, and coal may serve as an important source of organic substrates to the surrounding sediments. Coal can serve as a bioreactor in which complex coal macerals are degraded into simple, more labile molecules (e.g., acetate, H_2 , and CO_2) that become mobile as electron donors that can fuel methanogenesis [Strapoć *et al.*, 2008, 2011]. Peat prior to coal formation is a major source of dissolved organic carbon (DOC) into underlying sediments as well [Dalva and Moore, 1991]. During burial and through early coalification, the peat/lignite intervals at Site C0020 were a likely source of DOC to the surrounding low TOC sediments. Lignite within Unit III promotes methanogenesis and H_2 production [Inagaki *et al.*, 2015] and H_2 can serve as an electron donor for iron-reducing bacteria commonly found in estuaries [Caccavo *et al.*, 1992]. Within the C0020A sediments, average TOC of coal is 41 wt % while mudrocks, siltstone, and sandstone have 1.4, 0.43, and 0.26 wt %, respectively, [Expedition 337 Scientists, 2013]. Most coal beds within Unit III have little to no ferrimagnetic fraction, and likely had little Fe(III) present, thus presenting a physical separation between electron donors and electron acceptors necessary to fuel dissimilatory iron reduction. These coal beds are interbedded among siliciclastic sediments including massive fine-to-medium sand layers in the upper half of Unit III indicating an adjacent proximity of high-permeability sediments, initially (during early burial) likely to contain Fe(III) oxides, directly adjacent to a DOC and CH_4 sources.

In addition to the lignite as a source of electron donors, humic acids can facilitate iron reduction [Lovley *et al.*, 1996; Lovley and Blunt-Harris, 1999; Kappler *et al.*, 2004; Klüpfel *et al.*, 2014]. Humic acids comprise a significant fraction of lignite [e.g., Ibarra and Juan, 1985; Gonzalez-Vila, 1992, 1994; Cavani *et al.*, 2003; Allard, 2006] and can transfer electrons to iron oxides during acetate oxidation, alleviating the necessity of direct contact between Fe(III)-reducing bacteria and iron oxides [Lovley *et al.*, 1996]. The presence of peat/lignite in the subsiding environment at Site C0020A likely acted as a significant source of humic acids in the DOC to the surrounding sediments, thus enhancing iron reduction within intervals in pore water contact with the peat/coal intervals (Figure 9). Maximum methane content occurs within the coal beds (Figures 6 and 7) [Expedition 337 Scientists, 2013], including production by present-day methanogenesis [Inagaki *et al.*, 2015]. Methane oxidation may be coupled to iron reduction [Konhauser *et al.*, 2005; Thauer and Shima, 2008; Beal *et al.*, 2009; Segarra *et al.*, 2013; Riedinger *et al.*, 2014], suggesting methane exported from peat/lignite as a potential electron donor for iron reduction. Although both Units III and IV were deposited within a brackish/freshwater environment, only Unit III has numerous coal beds that can allow for a considerable source of humic acids and methane to the Fe(III)-bearing sediments. The presence of numerous coal beds in Unit III can explain why fine-grained authigenic magnetite is present in this unit, but not in Unit IV.

Within Unit III, the presence of unconsolidated sands suggests that fluid connectivity between coal beds and the surrounding sediments is maintained, but may be increasingly constricted with depth. Porosity decreases with depth from >0.8% at the top of overlying Hole C9001C to an average of 0.26% in Unit III [Aoike, 2007; Expedition 337 Scientists, 2013]. Within carbonate-cemented intervals of Unit III, porosity is further reduced to <0.15%. The decrease in porosity with depth due to compaction and diagenetic cements almost certainly limits permeability, thus impeding the connection between magnetite-sourced electron acceptors and coal-sourced electron donors. This presumed decrease in permeability, along with the decrease in cell concentration with depth [Inagaki *et al.*, 2015], suggests that the maximum rates for iron reduction likely occurred during shallow burial and declined with further burial depth.

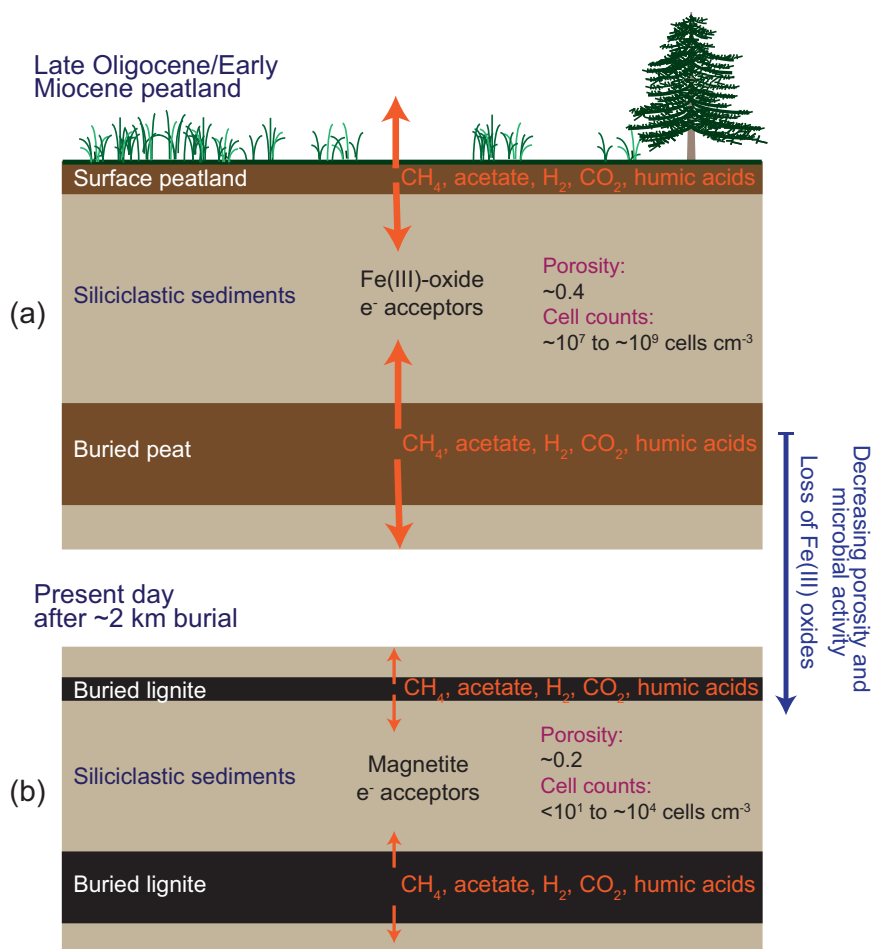


Figure 9. Schematic diagram illustrating the role that organic-rich peat/coal beds may play in promoting microbial iron reduction in the surrounding siliciclastic sediments of Unit III during burial. The coal can serve as an electron donor to the Fe(III) electron acceptors in the surrounding sediments via export of methane, DOC, and hydrogen, causing the formation of magnetite at the highest rate during early burial. With continued burial, depletion of amorphous iron oxides along with decreasing microbial activity and permeability likely slowed the rate of iron reduction. In the modern sequence, magnetite may be the main source of Fe(III) potentially available for iron reduction.

6.3.3. Potential for Continued Iron Reduction in the Deep Biosphere

As we discuss above, electron donors and Fe(III) electron acceptors were likely more readily available during early burial; however, the presence of indigenous terrestrial microbial communities within Unit III [Inagaki *et al.*, 2015] suggests the possibility that there may be continued iron reduction at depth, albeit at low rates. If iron reduction continues within the modern buried coal bed it is likely not a dominant process. Elevated H_2 concentrations at Site C0020 [Inagaki *et al.*, 2015] are consistent with observations that H_2 concentrations are lowest in sediments dominated by Fe(III) reduction and highest in those dominated by methanogenesis [Lovley and Goodwin, 1988; Lovley *et al.*, 1994], suggesting that methanogenesis is a dominant process.

Iron may play a role in the deep biosphere as a potential source of Fe(III) for iron reduction, possibly coupled to methane oxidation [Riedinger *et al.*, 2014]. Although iron reduction is thermodynamically more favorable than sulfate reduction and methanogenesis [Froelich *et al.*, 1979], Fe(III)-bearing iron oxides can persist during burial of sediments through the sulfidic and methanic zones [e.g., Kasten *et al.*, 1998; Riedinger *et al.*, 2005]. While the original depositional environment for Unit III is likely to have been rich in Fe(III) oxides, the lack of ascorbate extractable iron suggests that this source of Fe(III) has been depleted. Fe(III) is relatively immobile within a crystalline structure, and the presence of Fe(II) can limit the accessibility of Fe(III) thus limiting the bioavailability of magnetite Fe(III) for iron reducers [Roden and Zachara, 1996; Roden

and Urrutia, 1999]. However, Fe(III) and Fe(II) within magnetite have been shown to be bioavailable to both iron-reducing and iron-oxidizing bacteria, respectively [Byrne *et al.*, 2015].

Despite its crystalline structure, the presence of magnetite as the dominant magnetic mineral in the Site C0020A record suggests this mixed-valence iron oxide is a potential source of Fe(III) for present iron reduction in sediments offshore Shimokita within the deep biosphere. Reduction of magnetite-bound Fe(III) as an electron acceptor and magnetite dissolution have been observed in modern cultures of iron-reducing bacteria, and are shown to be energetically favorable under pH conditions typical of freshwater [Kostka and Nealson, 1995; Hori *et al.*, 2015]. In modern cultures of iron reducing bacteria with glucose or lactate as electron donors, magnetite loss occurs at rate on the order of 10^{-9} to 10^{-7} $\mu\text{mol h}^{-1} \text{cell}^{-1}$ [Nealson and Saffarini, 1994; Kostka and Nealson, 1995]. This rate of magnetite dissolution would consume all magnetite at Site C0020 over a period of tens of thousands to several million years. The fact that magnetite, even ultrafine magnetite, has remained the dominant magnetic mineral in these sediments since the Miocene, suggests that if magnetite is a source of Fe(III), iron reduction is proceeding at extremely low rates potentially limited by the accessibility of electron donors.

Other possible Fe(III)-bearing minerals present at Site C0020 include glauconite and smectite-group clays. Glauconite was commonly observed in smear slides in cores from Unit II and IV but was less common in Unit III [Expedition 337 Scientists, 2013]. Glombitza *et al.* [2016] suggest Fe(III) in glauconite may drive slow rates of sulfate recycling at Site C0020A. Clay mineralogy has not been characterized at C0020A, but smectite clay minerals are abundant in late Oligocene-early Miocene sediments at DSDP sites further offshore northern Honshu [Chamley *et al.*, 1986]. Iron-reducing bacteria (as well as sulfate-reducing bacteria and methanogens) have been shown to reduce Fe(III)-bearing clay minerals (e.g., nontronite) [e.g., Kostka *et al.*, 1999; Dong *et al.*, 2009; Pentráková *et al.*, 2013]. Furthermore, humic acids can stimulate the reduction of Fe(III)-bearing clays [Liu *et al.*, 2017]. Characterization of clay mineralogy at Site C0020 may further help elucidate the role of iron reduction in the deep biosphere.

7. Summary and Conclusions

We investigated changes in magnetic mineral assemblages and iron speciation across a transition in depositional and diagenetic environments at IODP Hole C0020A in order to identify the source of anomalous increases in magnetic susceptibility associated with a unit containing 0.3–7.3 m thick coal beds. Magnetic assemblages throughout the core are dominated by low-coercivity magnetite. In this record, cm-scale magnetic susceptibility increases are associated with organic-rich laminations in sandstone, siltstone, and shale lithologies within Unit III, a nearshore-to-intertidal coal-bearing depositional sequence. In Units II and IV, the linear loss of low-coercivity IRM during thermal demagnetization to 580°C suggests the presence of magnetite. Within the primary coal bearing intervals of Unit III (1925–1975 mbsf and 1979–1993 mbsf) partial or complete loss of low-coercivity IRM by 350–400°C indicates a secondary magnetite assemblage with a lower unblocking temperature due to decreased grain size. ARM and frequency dependence measurements support the presence of fine-grained SD and ultrafine SP magnetite. Measurements of $\delta^{56}\text{Fe}$ from total iron extractions also indicate the precipitation of authigenic magnetite. This phase of fine-grained magnetite is likely formed as extracellular precipitates during iron reduction. Interpretation of our rock magnetic record in the context of geochemical and microbiological results from IODP Expedition 337 [Expedition 337 Scientists, 2013; Inagaki *et al.*, 2015; Gross *et al.*, 2015] suggest that the depositional/diagenetic environment in which we observe fine-grained magnetite is conducive to microbial iron reduction. Peat/lignite in Unit III likely served as a source of electron donors (e.g., CH_4 and H_2) for iron reduction. Beginning early after deposition in this nearshore environment, microbial iron reduction most likely resulted in precipitation of authigenic magnetite by consumption of amorphous iron oxides. The proximity of the coalbeds as a source of electron acceptors and humic acid electron shuttles further enhanced iron reduction in Unit III. This process of microbial iron reduction may continue to occur with deeper burial and could continue today in the deep biosphere off Shimokita but at reduced rates due decreased microbial activity, reduced permeability, and the presence of only crystalline sources of Fe(III). Overall, these results suggest that peat/coal can facilitate iron reduction and magnetite formation in subsiding sediments.

Acknowledgments

We thank the Captain and crew of D/V *Chikyu* and the IODP Expedition 337 Scientists and technicians for core collection and initial onboard analysis. We are grateful for the support of IODP and the Ministry of Education, Culture, Sports, Science and Technology of Japan for supporting Expedition 337. We thank Lallan Gupta and the Kochi Core Center for collecting additional samples. This research was supported by two Post-Expedition Awards from the Consortium for Ocean Leadership-U.S. Science Support Program for S.P. and N.R., and this work was part of the dissertation of S.P. at the University of New Hampshire. We are grateful for helpful discussions with John Pohlman (USGS, Woods Hole), Jo Laird (UNH), and Julie Bryce (UNH) as part of the dissertation of S.P. We also thank Jo Laird for assistance with reflected light petrography. We thank Donggao Zhao and Brent Jackson at the UT-Austin Electron Microbeam Laboratory for assistance with EMPA analysis. We thank Christian März and two anonymous reviewers for their comments and suggestions that improved this paper. All data from this paper are available in the supporting information.

References

- Abrajevitch, A., L. M. Kondratyeva, E. M. Golubeva, K. Kodama, and R. S. Hori (2016), Magnetic properties of iron minerals produced by natural iron- and manganese-reducing groundwater bacteria, *Geophys. J. Int.*, *206*, 1340–1351.
- Akimoto, S., and T. Katsura (1959), Magneto-chemical study of generalized titanomagnetite in volcanic rocks, *J. Geomagn. Geoelectr.*, *10*, 69–90.
- Allard, B. (2006), A comparative study on the chemical composition of humic acids from forest soil, agricultural soil, and lignite deposit bound lipid, carbohydrate, and amino acid distributions, *Geoderma*, *130*, 77–96.
- Altschuler, Z. S., M. M. Schnepfe, C. C. Silber, and F. O. Simon (1983), Sulfur diagenesis in Everglades peat and origin of pyrite in coal, *Science*, *221*, 221–227.
- Aoi, K. (Ed.) (2007), CDEX laboratory operation report: CK06–06 D/V *Chikyu* shutdown cruise offshore Shimokita: Yokohama (CDEX-JAMSTEC), CDEX. [Available at http://sio7.jamstec.go.jp/JAMSTEC-exp-report/902/CK06-06_CR.pdf]
- Arnold, R. G., T. J. DiChristina, and M. R. Hoffman (1988), Reductive dissolution of Fe(III) oxides by *Pseudomonas* sp. 2000, *Biotechnol. Bioeng.*, *32*, 1081–1096.
- Arnold, G. L., S. Weyer, and A. D. Anbar (2004), Fe isotope variations in natural materials measured using high mass resolution multiple collector ICPMS, *Anal. Chem.*, *76*, 322–327.
- Arthur, M. A., R. Von Huene, and C. G. Adelseck (1980), Sedimentary evolution of the Japan fore-arc region off northern Honshu, Legs 56 and 57, Deep Sea Drilling Project, in *Initial Reports of the Deep Sea Drilling Project*, vol. 56/57, pp. 521–568, U.S. Gov. Print. Off., Washington, D. C.
- Atekwana, E. A., F. M. Mewafy, G. A. Aal, D. D. Werkema, A. Revil, and L. D. Slater (2014), High-resolution magnetic susceptibility measurements for investigating magnetic mineral formation during microbial mediated iron reduction, *J. Geophys. Res. Biogeosci.*, *119*, 80–94.
- Badesab, F., T. von Dobeneck, K. Bryan, H. Müller, R. M. Briggs, T. Frederichs, and E. Kroll (2012), Formation of magnetite-enriched zones in and offshore of a mesotidal estuarine lagoon: An environmental magnetic study of Tauranga Harbor and Bay of Plenty, New Zealand, *Geochem. Geophys. Geosyst.*, *13*, Q06012, doi:10.1029/2012GC004125.
- Bazylinski, D. A., and R. B. Frankel (2004), Magnetosome formation in prokaryotes, *Nat. Rev.*, *2*, 217–230.
- Bazylinski, D. A., R. B. Frankel, and H. W. Jannasch (1988), Anaerobic magnetite production by a marine, magnetotactic bacterium, *Nature*, *334*, 518–519.
- Beal, E. J., C. H. House, and V. J. Orphan (2009), Manganese- and iron dependent marine methane oxidation, *Science*, *325*, 184–187.
- Beard, B. L., C. M. Johnson, J. L. Skulan, K. H. Nealson, L. Cox, and H. Sun (2003), Application of Fe isotopes to tracing the geochemical and biological cycling of Fe, *Chem. Geol.*, *195*, 87–117.
- Bell, P. E., A. L. Mills, and J. S. Herman (1987), Biogeochemical conditions favoring magnetite formation during anaerobic iron reduction, *Appl. Environ. Microbiol.*, *53*, 2610–2616.
- Berner, R. A. (1981), A new geochemical classification of sedimentary environments, *J. Sediment. Petrol.*, *51*, 359–365.
- Blakemore, R. P. (1982), Magnetotactic bacteria, *Annu. Rev. Microbiol.*, *36*, 217–238.
- Bloemendal, J., J. W. King, A. Hunt, P. B. Demenocal, and A. Hayashida (1993), Origin of the sedimentary magnetic record at Ocean Drilling Program sites on the Owen Ridge, Western Arabian Sea, *J. Geophys. Res.*, *98*, 4199–4219.
- Byrne, J. M., N. Klueglein, C. Pearce, K. M. Rosso, E. Appel, and A. Kappler (2015), Redox cycling of Fe(II) and Fe(III) in magnetite by Fe-metabolizing bacteria, *Science*, *347*, 1473–1476.
- Caccavo, F., R. P. Blakemore, and D. R. Lovley (1992), A hydrogen-oxidizing, Fe(III)-reducing microorganism from the Great Bay Estuary, New Hampshire, *Appl. Environ. Microbiol.*, *58*, 3211–3216.
- Canfield, D. E. (1997), The geochemistry of river particulates from the continental USA: Major elements, *Geochim. Cosmochim. Acta*, *61*, 3349–3365.
- Canfield, D. E., and R. A. Berner (1987), Dissolution and pyritization of magnetite in anoxic marine sediments, *Geochim. Cosmochim. Acta*, *51*, 645–659.
- Canfield, D. E., and B. Thamdrup (2009), Towards a consistent classification scheme for geochemical environments, or, why we wish the term “suboxic” would go away, *Geobiology*, *7*, 385–392.
- Canfield, D. E., R. Raiswell, and S. Bottrell (1992), The reactivity of sedimentary iron minerals toward sulfide, *Am. J. Sci.*, *292*, 659–683.
- Cavani, L., C. Ciavatta, and C. Gessa (2003), Identification of organic matter from peat, Leonardite, and lignite fertilisers using humification parameters and electrofocusing, *Bioresour. Technol.*, *86*, 45–52.
- Chamley, H., J.-P. Cadet, and J. Charvet (1986), Nankai Trough and Japan Trench late Cenozoic paleoenvironments deduced from clay mineralogical data, in *Initial Reports of the Deep Sea Drilling Project*, vol. 87, pp. 633–642, U.S. Gov. Print. Off., Washington, D. C.
- Dalva, M., and T. R. Moore (1991), Sources and sinks of dissolved organic carbon in a forested swamp catchment, *Biogeochem.*, *15*, 1–19.
- Dearing, J. A., R. J. L. Dann, K. Hay, J. A. Lees, P. J. Loveland, B. A. Maher, and K. O. Grady (1996), Frequency-dependent susceptibility measurements of environmental materials, *Geophys. J. Int.*, *124*, 228–240.
- Dekkers, M. J. (1988), Magnetic properties of natural pyrrhotite Part I: Behaviour of initial susceptibility and saturation-magnetization-related rock-magnetic parameters in a grain-size dependent framework, *Phys. Earth Planet. Inter.*, *57*, 266–283.
- Dekkers, M. J., H. F. Passier, and M. A. A. Schoonen (2000), Magnetic properties of hydrothermally synthesized greigite (Fe₃S₄): II. High- and low-temperature characteristics, *Geophys. J. Int.*, *141*, 809–819.
- Devouard, B., M. Pósfai, X. Hua, D. A. Bazylinski, R. B. Frankel, and P. R. Buseck (1998), Magnetite from magnetotactic bacteria: Size distributions and twinning, *Am. Mineral.*, *83*, 1387–1398.
- D'Hondt, S., et al. (2004), Distributions of microbial activities in deep seafloor sediments, *Science*, *306*, 2216–2221.
- Dong, H., D. P. Jaisi, J. Kim, and G. Zhang (2009), Microbe-clay interactions, *Am. Mineral.*, *94*, 1505–1519.
- Dunlop, D. J. (1973a), Thermoremanent magnetization in submicroscopic magnetite, *J. Geophys. Res.*, *78*, 7602–7613.
- Dunlop, D. J. (1973b), Superparamagnetic and single-domain threshold sizes in magnetite, *J. Geophys. Res.*, *78*, 1780–1793.
- Elmore, R. D., and L. Crawford (1990), Remanence in authigenic magnetite: Testing the hydrocarbon-magnetite hypotheses, *J. Geophys. Res.*, *95*, 4539–4549.
- Elmore, R. D., M. H. Engel, L. Crawford, K. Nick, S. Imbus, and Z. Sofer (1997), Evidence for a relationship between hydrocarbons and authigenic magnetite, *Nature*, *325*, 428–430.
- Expedition 337 Scientists (2013), Site C0020, *Proc. Integrated Ocean Drill. Program*, *337*, 1–164, doi:10.2204/iodp.proc.337.103.2013.
- Fan, S.-M., W. J. Moxim, and H. Levy II (2006), Aeolian input of bioavailable iron to the ocean, *Geophys. Res. Lett.*, *33*, L07602, doi:10.1029/2005GL024852.

- Ferdelman, T. G. (1988), The distribution of sulfur, iron, manganese, copper and uranium in a salt marsh sediment core as determined by a sequential extraction method, MS thesis, 244 p., University of Delaware, Newark, Del.
- Froelich, P. N., G. P. Klinkhammer, M. L. Bender, N. A. Luetke, G. R. Heath, D. Cullen, P. Dauphin, D. Hammond, B. Hartman, and V. Maynard (1979), Early oxidation of organic matter in pelagic sediments of the eastern equatorial Atlantic: suboxic diagenesis, *Geochim. Cosmochim. Acta*, *43*, 1075–1090.
- Fu, Y., T. von Döbeneck, C. Franke, D. Heslop, and S. Kasten (2008), Rock magnetic identification and geochemical process models of greigite formation in Quaternary marine sediments from the Gulf of Mexico (IODP Hole U1319A), *Earth Planet. Sci. Lett.*, *275*, 233–245.
- Furukawa, Y., and H. L. Barnes (1995), Reactions forming pyrite from precipitated amorphous ferrous sulfide, in *Geochemical Transformation of Sedimentary Sulfur, ACS Symp. Ser.*, edited by M. A. Vairavamurthy and M. A. A. Schoonen, vol. 612, pp. 194–205, American Chemical Society, Washington, D. C.
- Garming, J. F. L., U. Bleil, and N. Riedinger (2005), Alteration of magnetic mineralogy at the sulfat-methane transition: Analysis of sediments from the Argentine continental slope, *Phys. Earth Planet. Inter.*, *151*, 290–308.
- Glombitza, C., R. R. Adhikari, N. Riedinger, W. P. Gilhooly, K.-U. Hinrichs, and F. Inagaki (2016), Microbial sulfate reduction potential in coal-bearing sediments down to ~2.5 km below the seafloor off Shimokita Peninsula, Japan, *Front. Microbiol.*, *7*, 1–15.
- Gonzalez-Vila, F. J., F. Martin, J. C. Del Rio, and R. Fründ (1992), Structural characteristics and geochemical significance of humic acids isolated from three Spanish lignite deposits, *Sci. Total Environ.*, *117/118*, 335–343.
- Gonzalez-Vila, F. J., J. C. del Rio, G. Almendros, and F. Martin (1994), Structural relationship between humic fractions from peat and lignites from the Miocene Granada basin, *Fuel*, *73*, 215–221.
- Gross, D., A. Bechtel, and G. Harrington (2015), Variability in coal facies as reflected by organic petrological and geochemical data in Cenozoic coal beds offshore Shimokita (Japan) – IODP 337, *Int. J. Coal Geol.*, *152B*, 63–79, doi:10.1016/j.coal.2015.10.007.
- Hall, F. R., and J. W. King (1989), Rock-magnetic stratigraphy of Site 645 (Baffin Bay) from ODP Leg 105, in *Proceedings of the Ocean Drilling Program, Scientific Results*, edited by S. P. Srivastava et al., vol. 105, pp. 843–859, Ocean Drill. Program, College Station, Tex.
- Hall, J. M., and D. Smeltzer (1980), Paleomagnetism of sediments, Sites 438 and 440, Deep Sea Drilling Project, in *Initial Reports of the Deep Sea Drilling Project*, vol. 57, pp. 1159–1166, U.S. Gov. Print. Off., Washington, D. C.
- Hall, S. A., and I. Evans (1995), Palaeomagnetic and rock magnetic properties of hydrocarbon reservoir rocks from the Permian Basin, south-eastern New Mexico, USA, *Geol. Soc. Spec. Publ.*, *98*, 79–95.
- Holmer, M., E. Kristensen, G. Banta, K. Hansen, M. H. Jensen, and N. Bussawarit (1994), Biogeochemical cycling of sulfur and iron in sediments of a south-east Asian mangrove, Phuket Island, Thailand, *Biogeochemistry*, *26*, 145–161.
- Hori, T., T. Aoyagi, H. Itoh, T. Narihiro, A. Oikawa, K. Suzuki, A. Ogata, M. W. Friedrich, R. Conrad, and Y. Kamagata (2015), Isolation of microorganisms involved in reduction of crystalline iron(III) oxides in natural environments, *Front. Microbiol.*, *6*, 386, 1–16, doi:10.3389/fmicb.2015.00386.
- Hornig, C. S., and A. P. Roberts (2006), Authigenic or detrital origin of pyrrhotite in sediments?: Resolving a paleomagnetic conundrum, *Earth Planet. Sci. Lett.*, *241*, 750–762.
- Hoshi, H., and Y. Teranishi (2007), Paleomagnetism of the Ishikoshi Andesite: A middle Miocene paleomagnetic pole for northeastern Japan and tectonic implications, *Earth Planets Space*, *59*, 871–878.
- Housen, B. A., and R. J. Musgrave (1996), Rock-magnetic signature of gas hydrates in accretionary prism sediments, *Earth Planet. Sci. Lett.*, *139*, 509–519.
- Hunger, S., and L. G. Benning (2007), Greigite: A true intermediate on the polysulfide pathway to pyrite, *Geochem. Trans.*, *8*, 1, doi:10.1186/1467-4866-8-1.
- Ibarra, J. V., and R. Juan (1985), Structural changes in humic acids during the coalification process, *Fuel*, *64*, 650–656.
- Inagaki, F., et al. (2015), Exploring the bottom of the deep biosphere ~2.5 km below the seafloor, *Science*, *349*, 420–424.
- Johnson, C. M., E. E. Roden, S. A. Welch, and B. L. Beard (2005), Experimental constraints on Fe isotope fractionation during magnetite and Fe carbonate formation coupled to dissimilatory hydrous ferric oxide reduction, *Geochim. Cosmochim. Acta*, *69*, 963–993.
- Just, J., M. J. Dekkers, T. vonDöbeneck, A. vanHoesel, and T. Bickert (2012), Signatures and significance of aeolian, fluvial, bacterial and diagenetic magnetic mineral fractions in Late Quaternary marine sediments off Gambia, NW Africa, *Geochem. Geophys. Geosyst.*, *13*, Q0A002, doi:10.1029/2012GC004146.
- Kanamatsu, T., and N. Niitsuma (2004), Rock magnetism and paleomagnetic stratigraphy of forearc sediments of the Japan Trench, ODP Sites 1150 and 1151, *Island Arc*, *13*, 180–190.
- Kanamatsu, T., J. M. Parés, and Y. Kitamura (2012), Pliocene shortening direction in Nankai Trough off Kumano, southwest Japan, Sites IODP C0001 and C0002, Expedition 315: Anisotropy of magnetic susceptibility analysis for paleostress, *Geochem. Geophys. Geosyst.*, *13*, Q0AD22, doi:10.1029/2011GC003782.
- Kappler, A., M. Benz, B. Schink, and A. Brune (2004), Electron shuttling via humic acids in microbial iron(III) reduction in a freshwater sediment, *FEMS Microbiol. Ecol.*, *47*, 85–92.
- Karlin, R. (1990), Magnetite diagenesis in marine sediments from the Oregon continental margin, *J. Geophys. Res.*, *95*, 4405–4419.
- Karlin, R., M. Lyle, and G. R. Heath (1987), Authigenic magnetite formation in suboxic marine sediments, *Nature*, *326*, 490–493.
- Kars, M., and K. Kodama (2015), Authigenesis of magnetic minerals in gas hydrate-bearing sediments in the Nankai Trough, offshore Japan, *Geochem. Geophys. Geosyst.*, *16*, 947–961, doi:10.1002/2014GC005614.
- Kasten, S., T. Freudenthal, F. X. Gingele, and H. D. Schulz (1998), Simultaneous formation of iron-rich layers at different redox boundaries in sediments of the Amazon deep-sea fan, *Geochim. Cosmochim. Acta*, *62*, 2253–2264.
- Kirschvink, J. L., and S.-B. R. Chang (1984), Ultrafine magnetite in deep-sea sediments: Possible bacterial magnetofossils, *Geology*, *12*, 559–562.
- Klüpfel, L., A. Piepenbrock, A. Kappler, and M. Sander (2014), Humic substances as fully regenerable electron acceptors in recurrently anoxic environments, *Nat. Geosci.*, *7*, 195–200.
- Komar, P. D. (1989), Physical processes of waves and currents and the formation of marine placers, *Rev. Aquat. Sci.*, *1*, 393–423.
- Konhauser, K. O., D. K. Newman, and A. Kappler (2005), The potential significance of microbial Fe(III) reduction during deposition of Precambrian banded iron formations, *Geobiology*, *3*, 167–177.
- Kostka, J. E., and G. W. Luther III (1994), Partitioning and speciation of solid phase iron in saltmarsh sediments, *Geochim. Cosmochim. Acta*, *58*, 1701–1710.
- Kostka, J. E., and K. H. Nealson (1995), Dissolution and reduction of magnetite by bacteria, *Environ. Sci. Technol.*, *29*, 2535–2540.
- Kostka, J. E., E. Haefele, R. Viehweger, and J. W. Stucki (1999), Respiration and dissolution of iron(III)-containing clay minerals by bacteria, *Environ. Sci. Technol.*, *33*, 3127–3133.

- Kruiver, P. P., M. J. Dekkers, and D. Heslop (2001), Quantification of magnetic coercivity components by analysis of acquisition curves of isothermal remanent magnetization, *Earth Planet. Sci. Lett.*, *189*, 269–276.
- Larrasoana, J. C., E. Gràcia, M. Garcés, R. J. Musgrave, E. Piñero, F. Martínez-Ruiz, and M. E. Vega (2006), Rock magnetic identification of magnetic iron sulfides and its bearing on the occurrence of gas hydrates, ODP Leg 204 (Hydrate Ridge), in *Proceedings of Ocean Drilling Program, Scientific Results*, edited by A. M. Tréhu et al., vol. 204, pp. 1–33, Ocean Drill. Program, College Station, Tex. [Available at http://www-odp.tamu.edu/publications/204_SR/VOLUME/CHAPTERS/111.PDF]
- Larrasoana, J. C., A. P. Roberts, R. J. Musgrave, E. Gràcia, E. Piñero, M. Vega, and F. Martínez-Ruiz (2007), Diagenetic formation of greigite and pyrrhotite in gas hydrate marine sedimentary systems, *Earth Planet. Sci. Lett.*, *261*, 350–366.
- Li, H., J. Peng, K. A. Weber, and Y. Zhu (2011), Phylogenetic diversity of Fe(III)-reducing microorganisms in rice paddy soil: Enrichment cultures with different short-chain fatty acids as electron acceptors, *J. Soils Sediments*, *11*, 1234–1242.
- Liu, G., S. Qiu, B. Liu, Y. Pu, Z. Gao, J. Wang, R. Jin, and J. Zhou (2017), Microbial reduction of Fe(III)-bearing clay minerals in the presence of humic acids, *Sci. Rep.*, *7*, 45354, 1–9, doi:10.1038/srep45354.
- Liu, Q., A. P. Roberts, J. C. Larrasoana, S. K. Banerjee, Y. Guyodo, L. Tauxe, and F. Oldfield (2012), Environmental magnetism: Principles and applications, *Rev. Geophys.*, *50*, RG4002, doi:10.1029/2012RG000393.
- Lovley, D. R. (1991a), Dissimilatory Fe(III) and Mn(IV) reduction, *Microbiol. Rev.*, *55*, 259–287.
- Lovley, D. R. (1991b), Magnetite formation during microbial dissimilatory iron reduction, in *Iron Biominerals*, edited by R. B. Frankel and R. P. Blakemore, pp. 155–166, Plenum, New York.
- Lovley, D. R., and F. H. Chapelle (1995), Deep surface microbial processes, *Rev. Geophys.*, *33*, 365–381.
- Lovley, D. R., and E. L. Blunt-Harris (1999), Role of humic-bound iron as an electron transfer agent in dissimilatory Fe(III) reduction, *Appl. Environ. Microbiol.*, *65*, 4252–4254.
- Lovley, D. R., and S. Goodwin (1988), Hydrogen concentrations as an indicator of the predominant terminal electron accepting reactions in aquatic sediments, *Geochim. Cosmochim. Acta*, *52*, 2993–3003.
- Lovley, D. R., and E. J. P. Phillips (1986), Availability of ferric iron for microbial reduction in bottom sediments of the freshwater tidal Potomac River, *Appl. Environ. Microbiol.*, *52*, 751–757.
- Lovley, D. R., J. F. Stoltz, G. L. Nord, and E. J. P. Phillips (1987), Anaerobic production of magnetite by a dissimilatory iron-reducing microorganism, *Nature*, *330*, 252–254.
- Lovley, D. R., F. H. Chapelle, and J. C. Woodward (1994), Use of dissolved H₂ concentrations to determine the distribution of microbially catalyzed redox reactions in anoxic ground water, *Environ. Sci. Technol.*, *28*, 1005–1210.
- Lovley, D. R., J. D. Coates, E. L. Blunt-Harris, E. J. P. Phillips, and J. C. Woodward (1996), Humic substances as electron acceptors for microbial respiration, *Nature*, *382*, 445–448.
- Lowrie, W. (1990), Identification of ferromagnetic minerals in a rock by coercivity and unblocking temperature properties, *Geophys. Res. Lett.*, *17*, 159–162.
- Ludwig, P., R. Egli, S. Bishop, V. Chernenko, T. Frederichs, G. Rugel, S. Merchel, and M. J. Orgeira (2013), Characterization of primary and secondary magnetite in marine sediment by combining chemical and magnetic unmixing techniques, *Global Planet. Change*, *110*, 321–329.
- Mahowald, N. M., A. R. Baker, G. Bergametti, N. Brooks, R. A. Duce, T. D. Jickells, N. J. Kubilay, J. M. Prospero, and I. Tegen (2005), Atmospheric global dust cycle and iron inputs to the ocean, *Global Biogeochem. Cycles*, *19*, GB4025, doi:10.1029/2004GB002402.
- Mandernack, K. W., D. A. Bazylinski, W. A. Shanks, and T. D. Bullen (1999), Oxygen and iron isotope studies of magnetite produced by magnetotactic bacteria, *Science*, *285*, 1892–1896.
- Maynard, J. B. (1982), Extension of Berner's "new geochemical classification of sedimentary environments" to ancient environments, *J. Sediment. Petrol.*, *52*, 1325–1331.
- McCabe, C., R. Sassen, and B. Saffer (1987), Occurrence of secondary magnetite within biodegraded oil, *Geology*, *15*, 7–10.
- Mewafy, F. M., E. A. Atekwana, D. D. Werkema, L. D. Slater, D. Ntarlagiannis, A. Revil, M. Skold, and G. N. Delin (2011), Magnetic susceptibility as a proxy for investigating microbially mediated iron reduction, *Geophys. Res. Lett.*, *38*, L21402, doi:10.1029/2011GL049271.
- Mortimer, R. J. G., and M. L. Coleman (1997), Microbial influence on the oxygen isotopic composition of diagenetic siderite, *Geochim. Cosmochim. Acta*, *61*, 1705–1711.
- Moskowitz, B. M., R. B. Frankel, D. A. Bazylinski, H. W. Jannasch, and D. R. Lovley (1989), A comparison of magnetite particles produced anaerobically by magnetotactic and dissimilatory iron-reducing bacteria, *Geophys. Res. Lett.*, *16*, 665–668.
- Moskowitz, B. M., R. B. Frankel, and D. A. Bazylinski (1993), Rock magnetic criteria for the detection of biogenic magnetite, *Earth Planet. Sci. Lett.*, *120*, 283–300.
- Musgrave, R. J., N. L. Bangs, J. C. Larrasoana, E. Gràcia, J. A. Hollamby, and M. E. Vega (2006), Rise of the base of the gas hydrate zone since the last glacial recorded by rock magnetism, *Geology*, *34*, 117–120.
- Nealson, K. H., and D. Saffarini (1994), Iron and manganese in anaerobic respiration: Environmental significance, physiology, and regulation, *Annu. Rev. Microbiol.*, *48*, 311–343.
- Neretin, L. N., M. E. Böttcher, B. B. Jørgensen, I. I. Volkov, H. Lüschen, and K. Higenfeldt (2004), Pyritization processes and greigite formation in the advancing sulfidization front in the Upper Pleistocene sediments of the Black Sea, *Geochim. Cosmochim. Acta*, *68*, 2081–2093.
- Niitsuma, N. (1986), Paleomagnetic results, Nankai Trough and Hapan Trench, Deep Sea Drilling Project Leg 87, in *Initial Reports of the Deep Sea Drilling Project*, vol. 87, pp. 757–786, U.S. Gov. Print. Off., Washington, D. C.
- Ohba, T., Y. Kimura, and H. Fujimaki (2007), High-magnesian andesite produced by two-stage magma mixing: A case study from Hachiman-tai, northern Honshu, Japan, *J. Petrol.*, *48*, 627–645.
- Pan, Y., R. Zhu, and J. Ping (1999), Mineralogical alteration of thermally treated siderite in air: Mössbauer spectroscopy results, *Chin. Sci. Bull.*, *44*, 1712–1717.
- Pan, Y., R. Zhu, S. K. Banerjee, J. Gill, and Q. Williams (2000), Rock magnetic properties related to thermal treatment of siderite: Behavior and interpretation, *J. Geophys. Res.*, *105*, 783–794.
- Pan, Y., R. Zhu, Q. Liu, and M. Jackson (2002), Low-temperature magnetic behavior related to thermal alteration of siderite, *Geophys. Res. Lett.*, *29*(3), 2087, doi:10.1029/2002GL016021.
- Pentáková, L., K. Su, M. Pentrák, and J. W. Stucki (2013), A review of microbial redox interactions with structural Fe in clay minerals, *Clay Minerals*, *48*, 543–560.
- Pérez-Pérez, A. R., H. E. Romero, and L. D'Onofrio (2016), A statistical and graphical workflow for the analysis of magnetic susceptibility data from drill cuttings in a hydrocarbon exploration setting, *Geophysics*, *81*, J35–J46.
- Peters, C., and M. J. Dekkers (2003), Selected room temperature magnetic parameters as a function of mineralogy, concentration and grain size, *Phys. Chem. Earth*, *28*, 659–667.

- Phillips, M. P., D. M. Harwood, and G. J. Harrington (2016), Neogene and Early Pleistocene diatom biostratigraphy and age synthesis of Site C9001/C0020, Northwest Pacific, *Mar. Micropaleontol.*, *128*, 39–49.
- Postma, D. (1982), Pyrite and siderite formation in brackish and swamp sediments, *Am. J. Sci.*, *282*, 1151–1183.
- Poulton, S. W., and D. E. Canfield (2005), Development of a sequential extraction procedure for iron: Implications for iron partitioning in continentally derived particulates, *Chem. Geol.*, *214*, 3703–3713.
- Poulton, S. W., M. D. Krom, and R. Raiswell (2004), A revised scheme for the reactivity of iron (oxyhydr)oxide minerals towards dissolved sulfide, *Geochim. Cosmochim. Acta*, *68*, 3703–3715.
- Pye, K., J. A. D. Dickson, N. Schiavon, M. L. Coleman, and M. Cox (1990), Formation of siderite-Mg-calcite-iron sulphide concretions in intertidal marsh and sandflat sediments, north Norfolk, England, *Sedimentology*, *37*, 325–343.
- Quinton, E. E., D. E. Dahms, and C. E. Geiss (2011), Magnetic analyses of soils from Wyoming, constrain rates and pathways of magnetic enhancement for soils from semiarid climates, *Geochem. Geophys. Geosyst.*, *12*, Q07Z30, doi:10.1029/2011GC003728.
- Raiswell, R., and D. E. Canfield (1998), Sources of iron for pyrite formation in marine sediments, *Am. J. Sci.*, *298*, 219–245.
- Raiswell, R., D. E. Canfield, and R. A. Berner (1994), A comparison of iron extraction methods for the determination of degree of pyritisation and the recognition of iron-limited pyrite formation, *Chem. Geol.*, *111*, 101–110.
- Raiswell, R., H. P. Vu, L. Brinza, and L. G. Benning (2010), The determination of labile Fe in ferrihydrite by ascorbic acid extraction: Methodology, dissolution kinetics and loss of solubility with age and dewatering, *Chem. Geol.*, *278*, 70–79.
- Razjigaeva, N. G., and V. V. Naumova (1992), Trace element composition of detrital magnetite from coastal sediments of northwestern Japan Sea for provenance study, *J. Sediment. Res.*, *62*, 802–809.
- Regalla, C., D. M. Fisher, E. Kirby, and K. P. Furlong (2013), Relationship between outer forearc subsidence and plate boundary kinematics along the Northeast Japan convergent margin, *Geochem. Geophys. Geosyst.*, *14*, 5227–5243.
- Richter, T. O., S. Lassen, T. C. E. van Weering, and H. de Haas (2001), Magnetic susceptibility patterns and provenance of ice-rafted material at Feni Drift, Rockall Trough: Implications for the history of the British-Irish ice sheet, *Mar. Geol.*, *173*, 37–54.
- Riedinger, N., K. Pfeifer, S. Kasten, J. F. L. Garming, C. Vogt, and C. Hensen (2005), Diagenetic alteration of magnetic signals by anaerobic oxidation of methane related to a change in sedimentation rate, *Geochim. Cosmochim. Acta*, *69*, 4117–4126.
- Riedinger, N., B. Brunner, M. J. Formolo, E. Solomon, S. Kasten, M. Strasser, and T. G. Ferdelman (2010), Oxidative sulfur cycling in the deep biosphere of the Nankai Trough, Japan, *Geology*, *38*, 851–854.
- Riedinger, N., M. J. Formolo, T. W. Lyons, S. Henkel, A. Beck, and S. Kasten (2014), An inorganic geochemical argument for coupled anaerobic oxidation of methane and iron reduction in marine sediments, *Geobiology*, *12*, 172–181.
- Roberts, A. P. (1995), Magnetic properties of sedimentary greigite (Fe₃S₄), *Earth Planet. Sci. Lett.*, *134*, 227–236.
- Roberts, A. P. (2015), Magnetic mineral diagenesis, *Earth Sci. Rev.*, *151*, 1–47, doi:10.1016/j.earscirev.2015.09.010.
- Roberts, A. P., F. Florindo, G. Villa, L. Chang, L. Jovane, S. M. Bohaty, J. C. Larrasoana, D. Heslop, and J. D. FitzGerald (2011), Magnetotactic bacterial abundance in pelagic marine environments is limited by organic carbon flux and availability of dissolved iron, *Earth Planet. Sci. Lett.*, *310*, 441–442.
- Robinson, S. G. (1986), The late Pleistocene palaeoclimatic record of North Atlantic deep-sea sediments revealed by mineral-magnetic measurements, *Phys. Earth Planet. Inter.*, *42*, 22–47.
- Roden, E. E., and J. M. Zachara (1996), Microbial reduction of crystalline iron(III) oxides: Influence of oxide surface area and potential for cell growth, *Environ. Sci. Technol.*, *30*, 1618–1628.
- Roden, E. E., and M. M. Urrutia (1999), Ferrous iron removal promotes microbial reduction of crystalline iron(III) oxides, *Environ. Sci. Technol.*, *33*, 1847–1853.
- Rouxel, O., E. Sholkovitz, M. Charette, and K. J. Edwards (2008), Iron isotope fractionation in subterranean estuaries, *Geochim. Cosmochim. Acta*, *72*, 3413–3430.
- Rowan, C. J., and A. P. Roberts (2006), Magnetite dissolution, diachronous greigite formation, and secondary magnetizations from pyrite oxidation: Unravelling complex magnetizations in Neogene marine sediments from New Zealand, *Earth Planet. Sci. Lett.*, *241*, 119–137.
- Sacks, I. S., and K. Suyehiro (2003), Leg 186 synthesis: Drilling the forearc of the northeast Japan arc—Causes and effects of subduction plate coupling over 20 m.y., in *Proceedings of the Ocean Drilling Program, Scientific Results*, edited by K. Suyehiro et al., vol. 186, pp. 1–27, Ocean Drill. Program, College Station, Tex. [Available at http://www-odp.tamu.edu/publications/186_SR/VOLUME/SYNTH/SYNTH.PDF]
- Sakuyama, M., and R. W. Nesbitt (1986), Geochemistry of the Quaternary volcanic rocks of the northeast Japan Arc, *J. Volcanol. Geotherm. Res.*, *29*, 413–450.
- Sassen, R., C. McCabe, J. R. Kyle, and E. W. Chinn (1989), Deposition of magnetic pyrrhotite during alteration of crude oil and reduction of sulfate, *Org. Geochem.*, *14*, 381–392.
- Saunders, D. F., K. R. Burson, and C. K. Thompson (1991), Observed relation of soil magnetic susceptibility and soil gas hydrocarbon analyses to subsurface hydrocarbon accumulations, *Am. Assoc. Pet. Geol. Bull.*, *75*, 389–408.
- Schön, J. H. (2004), *Physical Properties of Rocks: Fundamentals and Principles of Petrophysics*, 600 p., Pergamon, Oxford, U. K.
- Segarra, K. E. A., C. Comerford, J. Slaughter, and S. B. Joye (2013), Impact of electron acceptor availability on the anaerobic oxidation of methane in coastal freshwater and brackish wetland sediments, *Geochim. Cosmochim. Acta*, *115*, 15–30.
- Severmann, S., C. M. Johnson, B. L. Beard, and J. McManus (2006), The effect of early diagenesis on the Fe isotope compositions of porewaters and authigenic minerals in continental margin sediments, *Geochim. Cosmochim. Acta*, *70*, 2006–2022.
- Slingerland, R., and N. D. Smith (1986), Occurrence and formation of water-laid placers, *Annu. Rev. Earth Planet. Sci.*, *14*, 113–147.
- Smirnov, A. V., and J. A. Tarduno (2000), Low-temperature magnetic properties of pelagic sediments (Ocean Drilling Program Site 805C): Tracers of magnetization and magnetic mineral reduction, *J. Geophys. Res.*, *105*, 16,457–16,471.
- Steinmann, P., and W. Shotyk (1997), Chemical composition, pH, and redox state of sulfur and iron in complete vertical porewater profiles from two Sphagnum peat bogs, Jura Mountains, Switzerland, *Geochim. Cosmochim. Acta*, *61*, 1143–1163.
- Strapoć, D., et al. (2008), Methane-producing microbial community in a coal bed of the Illinois Basin, *Appl. Environ. Microbiol.*, *74*, 2424–2432.
- Strapoć, D., M. Mastalerz, K. Dawson, J. Macalady, A. V. Callaghan, B. Wawrik, C. Turich, and M. Ashby (2011), Biogeochemistry of microbial coal-bed methane, *Annu. Rev. Earth Planet. Sci.*, *39*, 617–656.
- Suzuki, T. (2008), Analysis of titanomagnetite within weathered middle Pleistocene KMT tephra and its application for fluvial terrace chronology, Kanto Plain, central Japan, *Quat. Int.*, *178*, 119–127.
- Sweeney, R. E., and I. R. Kaplan (1973), Pyrite framboid formation: Laboratory synthesis and marine sediments, *Econ. Geol.*, *68*, 618–634.
- Takagi, T. (2004), Origin of magnetite- and ilmenite-series granitic rocks in the Japan Arc, *Am. J. Sci.*, *304*, 169–202.
- Taylor, S. R., and S. M. McLennan (1985), *The Continental Crust: Its Composition and Evolution: An Examination of the Geochemical Record Preserved in Sedimentary Rocks*, 312 p., Blackwell, Oxford.

- Tessier, A., P. G. C. Campbell, and M. Bisson (1979), Sequential extraction procedure for the speciation of particulate trace metals, *Anal. Chem.*, *51*, 844–851.
- Thauer, R. K., and S. Shima (2008), Methane as fuel for anaerobic microorganisms, *Ann. New York Acad. Sci.*, *1125*, 158–170.
- Tsuse, A. (1962), Genetic considerations of magnetite and pyrrhotite in pyritic deposits, Yanahara District, southwestern Japan, *Econ. Geol.*, *57*, 696–977.
- Ünal, B., V. R. Perry, M. Sheth, V. Gomez-Alvarez, K.-J. Chin, and K. Nüsslein (2012), Trace elements affect methanogenic activity and diversity in enrichments from subsurface coal bed produced water, *Front. Microbiol.*, *3*, 1–14.
- Verosub, K. L., and A. P. Roberts (1995), Environmental magnetism: Past, present, and future, *J. Geophys. Res.*, *100*, 2175–2192.
- Vigliotti, L. (1997), Magnetic properties of light and dark sediment layers from the Japan Sea: Diagenetic and paleoclimatic implications, *Quat. Sci. Rev.*, *16*, 1093–1114.
- Von Huene, R., M. Langseth, N. Nasu, and H. Okada (1982), A summary of Cenozoic tectonic history along the IPOD Japan Trench transect, *Geol. Soc. Am. Bull.*, *93*, 829–846.
- Waters, K. E., N. A. Rowson, R. W. Greenwood, and A. J. Williams (2008), The effect of heat treatment on the magnetic properties of pyrite, *Miner. Eng.*, *21*, 679–682.
- Winklhofer, M., K. Fabian, and F. Heider (1997), Magnetic blocking temperatures of magnetite calculated with a three-dimensional micro-magnetic model, *J. Geophys. Res.*, *102*, 22,695–22,709.
- Xu, W., D. R. Peacor, W. A. Dollase, R. Van Der Voo, and R. Beaubouef (1997), Transformation of titanomagnetite to titanomaghemite: A slow, two-step oxidation-ordering process in MORB, *Am. Mineral.*, *82*, 1101–1110.
- Zhao, X., H. Oda, H. Wu, T. Yamamoto, Y. Yamamoto, Y. Yamamoto, T. Nakajima, Y. Kitamura, and T. Kanamatsu (2013), Magnetostratigraphic results from sedimentary rocks of IODP's Nankai Trough Seismogenic Zone Experiment (NanTroSEIZE) Expedition 322, *Geol. Soc. Spec. Publ.*, *373*, 191–243.